

Wrinkled tori and bursts due to resonant temporal forcing

Jeff Moehlis*, Edgar Knobloch

Department of Physics, University of California, Berkeley, CA 94720, USA

Received 26 June 2000; received in revised form 6 November 2000; accepted 5 January 2001

Communicated by F.H. Busse

Abstract

The effect of resonant temporal forcing on a system undergoing a Hopf bifurcation with D_4 (square) symmetry is studied. The forcing breaks the continuous normal form symmetry of the governing amplitude equations, but the D_4 symmetry is preserved. For this system, it is shown that bursts with very large dynamic range may occur. The bursts are associated with visits near solutions “at infinity”, and are related to those found previously for the Hopf bifurcation with broken D_4 symmetry [Moehlis and Knobloch, *Physica D* 135 (2000) 263]. The regime in which an attracting quasiperiodic solution that exists in the absence of forcing “wrinkles” into chaos as the amplitude of the forcing increases is investigated in detail. The overall behavior is governed by the approach of the resulting attractor to solutions at infinity. Windows with stable periodic solutions are found and associated with the traversal in parameter space through Arnol’d tongues. Other aspects of the dynamics are related to the presence of a new type of gluing bifurcation (which we call a “supergluing bifurcation”). © 2001 Elsevier Science B.V. All rights reserved.

PACS: 05.45.-b; 47.20.Ky; 47.52.+j; 47.54.+r

Keywords: Wrinkled tori; Bursts; Resonant temporal forcing

1. Introduction

The introduction of small symmetry-breaking perturbations can be responsible for complex dynamics in a system that would otherwise behave in a regular manner. Effects of such symmetry-breaking include the appearance of new solutions which have no analog in the fully symmetric system, and the introduction of global bifurcations which may be responsible for the appearance of chaotic dynamics and bursts with very large dynamic range [1–8]. For systems undergoing a Hopf bifurcation, temporal forcing of the system breaks the continuous normal form symmetry of the governing amplitude equations. If the forcing frequency is near a strong resonance with the Hopf frequency, the presence of forcing may have a large impact on the behavior of the system even if its amplitude is small [9–14]. In this paper, we consider the effect of resonant temporal forcing on a system undergoing a Hopf bifurcation with D_4 (square) symmetry from this point of view. In the absence of forcing this problem is described by a normal form

* Corresponding author. Present address: Program in Applied and Computational Mathematics, Princeton University, Princeton, NJ 08544, USA.

E-mail address: jmoehlis@math.princeton.edu (J. Moehlis).

with the symmetry $D_4 \times S^1$. In earlier work [6–8] we showed that breaking the $D_4 \times S^1$ symmetry down to $D_2 \times S^1$ could, in appropriate circumstances, result in bursts of large dynamic range near threshold of the primary instability, and showed that this behavior is a consequence of the formation of heteroclinic connections to “infinity” due to the symmetry breaking. In the present paper, we show that a similar mechanism operates in the case when the symmetry $D_4 \times S^1$ is broken down to D_4 by parametric (subharmonic) forcing. Although the basic mechanisms leading to the appearance of bursts in these two cases are largely similar in that both involve heteroclinic connections to infinity, the parametric forcing case introduces several interesting wrinkles on the mechanism described in [7,8].

We begin by deriving the basic equations we study, and then describe in some detail their properties for a specific (but generic) set of coefficient values. This work is almost entirely numerical, largely because the dynamical system we study is four-dimensional and not three-dimensional as in [7,8]. This is in turn a consequence of breaking a continuous symmetry as opposed to a discrete one. The paper concludes with a brief conclusion and a remark on a new type of gluing bifurcation that plays a role in some of the dynamics we describe.

2. The normal form equations

We consider finite-dimensional dissipative parametrically driven systems of the form

$$\frac{d\mathbf{U}}{dt} = L_\epsilon \mathbf{U} + \mathbf{f}(\mathbf{U}) + \delta \mathbf{F}(\mathbf{U}, t), \quad \mathbf{U} \in \mathbb{R}^N, \quad (1)$$

where L_ϵ is an $N \times N$ matrix that has a pair of (possibly degenerate) purely imaginary eigenvalues when $\epsilon = 0$, \mathbf{f} is a nonlinear vector-valued function of the dependent variables \mathbf{U} , δ denotes the strength of the forcing, and

$$\mathbf{F}\left(\mathbf{U}, t + \frac{2\pi}{\omega_e}\right) = \mathbf{F}(\mathbf{U}, t).$$

Here $2\pi/\omega_e$ is the period of the parametric forcing. Equations of this type describe the effect of weak ($\delta \ll 1$) periodic forcing on continuum systems in bounded domains or with periodic boundary conditions near a spontaneous Hopf bifurcation, and arise as the result of a truncation of a modal expansion. In this case the vector \mathbf{U} represents the vector of modal amplitudes. Systems of this type that have been studied experimentally include binary fluid convection [15] and the Taylor–Dean system [16]. A particularly important application arises in electroconvection, namely the formation of spatial patterns in nematic liquid crystals subjected to an oscillating vertical electric field [14,15,17]. In the following, we are interested in understanding the interplay between the two small parameters in the system, the parameter ϵ that measures the distance from the spontaneous bifurcation and the parameter δ that specifies the forcing amplitude. It is this interplay that is responsible for the novel dynamical behavior described below.

In the presence of spatial symmetries, the system (1) will be equivariant with respect to an appropriate action of the corresponding symmetry group; this action can be deduced from the action of the symmetry group on the spatial modes used in the expansion. In such cases the algebraic multiplicity of the purely imaginary eigenvalues present at $\epsilon = 0$ may be greater than 1. A typical example relevant to the present paper is provided by a continuum system undergoing a (symmetry-breaking) oscillatory instability in a domain of square cross-section. In the following we assume that the symmetry of the problem is not changed when δ becomes nonzero.

At $\epsilon = 0$ the system (1) can be reduced to a simpler form, called the normal form, describing the evolution of the system on the center manifold. The normal form contains only resonant terms, i.e., terms which cannot be eliminated through a near-identity change of variables. For nonautonomous systems of the form (1) this equation takes the form

$$\frac{d\mathbf{z}}{dt} = \mathcal{L}\mathbf{z} + \mathbf{N}(\mathbf{z}, t, \delta), \quad \mathbf{z} \in \mathbb{R}^M, \quad M \leq N, \quad (2)$$

where \mathcal{L} is the projection of L_0 onto the center manifold coordinates \mathbf{z} (i.e., the eigenvalues of \mathcal{L} all lie on the imaginary axis), and [18]

$$\frac{d}{dt}[\exp(\mathcal{L}^\dagger t)\mathbf{N}(\exp(-\mathcal{L}^\dagger t)\mathbf{z}, t, \delta)] = 0. \quad (3)$$

Here \mathcal{L}^\dagger is the adjoint (transpose and complex conjugate) of \mathcal{L} . The variables \mathbf{z} and t in Eq. (3) are treated as independent variables. A comparison with the normal form of autonomous systems [19] reveals that all the terms that appear in the normal form in the *absence* of forcing ($\delta = 0$) remain when forcing is present ($\delta \neq 0$). However, *additional* terms due to the forcing may also be present, indicating that temporal forcing may indeed be viewed as a symmetry-breaking perturbation, i.e., in the presence of forcing the continuous time-translation symmetry present in the normal form for the Hopf bifurcation is broken because the system is only unchanged under the *discrete* time-translations $t \rightarrow t + (2\pi/\omega_e)j$, where j is an integer.

The present paper focuses on a specific example of the above set-up. We consider the case of a system which undergoes a Hopf bifurcation with D_4 (square) symmetry. In the *absence* of external temporal forcing, the normal form equations governing the evolution of the complex amplitudes z_+ and z_- are equivariant with respect to the group $D_4 \times S^1$, where D_4 is generated by the operations [20]

$$\kappa_1 : (z_+, z_-) \rightarrow (z_+, -z_-), \quad \kappa_2 : (z_+, z_-) \rightarrow (z_-, z_+),$$

and S^1 is the normal form symmetry

$$N_\sigma : (z_+, z_-) \rightarrow e^{i\sigma}(z_+, z_-), \quad \sigma \in [0, 2\pi).$$

Suppose that the Hopf frequency at onset is ω_0 , and consider the effect of temporally periodic forcing with angular frequency ω_e . Making use of the symmetry κ_2 , the normal form equation in the *presence* of forcing is

$$\frac{dz_\pm}{dt} = i\omega_0 z_\pm + N(z_\pm, z_\mp, t),$$

where from Eq. (3)

$$\frac{d}{dt}[e^{-i\omega_0 t} N(e^{i\omega_0 t} z_+, e^{i\omega_0 t} z_-, t)] = 0.$$

Letting

$$N(z_+, z_-, t) = \sum_{l=-\infty}^{\infty} \sum_{\alpha, \beta, \gamma, \mu \geq 0} N_{l\alpha\beta\gamma\mu} z_+^\alpha \bar{z}_+^\beta z_-^\gamma \bar{z}_-^\mu e^{il\omega_e t},$$

we conclude that $N_{l\alpha\beta\gamma\mu} = 0$ for all l, α, β, γ , and μ such that

$$\omega_e l + (\alpha - \beta + \gamma - \mu - 1)\omega_0 \neq 0.$$

Note that the terms in the normal form must also be consistent with the other symmetries of the system. For $l = 0$, we obtain the terms in the normal form which are present in the absence of forcing (cf. [20]).

We now restrict attention to the strong resonance $\omega_e \approx 2\omega_0$. The possible additional terms which are of lowest order in the amplitudes z_+ and z_- for which $N_{l\alpha\beta\gamma\mu}$ can be nonzero are then

$$\begin{aligned} (l, \alpha, \beta, \gamma, \mu) = (1, 0, 1, 0, 0) : \dot{z}_+ &\sim \bar{z}_+ e^{i\omega_e t}, \quad \dot{z}_- \sim \bar{z}_- e^{i\omega_e t}, \\ (l, \alpha, \beta, \gamma, \mu) = (1, 0, 0, 0, 1) : \dot{z}_+ &\sim \bar{z}_- e^{i\omega_e t}, \quad \dot{z}_- \sim \bar{z}_+ e^{i\omega_e t}. \end{aligned}$$

It is readily shown that the first case is consistent with the symmetry κ_1 while the second case is not. Thus the simplest system that describes the effect of parametric forcing on the Hopf bifurcation with D_4 symmetry takes the form

$$\begin{aligned}\frac{dz_+}{dt} &= i\omega_0 z_+ + f \bar{z}_+ e^{i\omega_e t} + A(|z_+|^2 + |z_-|^2)z_+ + B|z_+|^2 z_+ + C \bar{z}_+ z_-^2, \\ \frac{dz_-}{dt} &= i\omega_0 z_- + f \bar{z}_- e^{i\omega_e t} + A(|z_+|^2 + |z_-|^2)z_- + B|z_-|^2 z_- + C \bar{z}_- z_+^2,\end{aligned}$$

and includes the lowest order term due to the forcing and the cubic terms that are present even when $\delta = 0$ [8]. Higher order terms in the forcing amplitude may introduce additional phenomena, but the present system is the simplest that incorporates both the Hopf bifurcation and effects of parametric forcing. Moreover, the resulting equations can also be derived by a systematic *asymptotic* procedure as discussed in [8].

The coefficients A, B, C are complex ($A = A_R + iA_I$, etc.) and f can without loss of generality be taken to be real. Letting $z_{\pm} = e^{i\omega_e t/2} \tilde{z}_{\pm}$, dropping the tildes, and unfolding the equations by introducing the parameter λ to represent the (scaled) distance from the Hopf bifurcation in the absence of forcing, we obtain the autonomous normal form equations

$$\frac{dz_+}{dt} = (\lambda + i\omega)z_+ + f \bar{z}_+ + A(|z_+|^2 + |z_-|^2)z_+ + B|z_+|^2 z_+ + C \bar{z}_+ z_-^2, \quad (4)$$

$$\frac{dz_-}{dt} = (\lambda + i\omega)z_- + f \bar{z}_- + A(|z_+|^2 + |z_-|^2)z_- + B|z_-|^2 z_- + C \bar{z}_- z_+^2. \quad (5)$$

Here $\omega \equiv \omega_0 - \frac{1}{2}\omega_e$ is called the detuning, and f is related to the strength of the forcing. It is readily shown that Eqs. (4) and (5) also apply to the case that $\omega_e \approx \omega_0$; in this case the detuning is $\omega \equiv \omega_0 - \omega_e$. In general this detuning is a function of λ , since away from onset the natural frequency $\omega_0 = \omega_0(\lambda)$. In these equations all quantities are formally of order one, cf. [8].

Eqs. (4) and (5) are equivariant with respect to the group $D_4 = \langle \kappa_1, \kappa_2 \rangle$, although they are not the most general such equations because the S^1 normal form symmetry is broken only at leading order. The most detailed study of these equations thus far is that given in [14] in the context of electroconvection, and we refer the reader to this paper for a summary of the elementary solutions and their bifurcations. In this paper, we investigate some of the novel dynamical behavior in these equations that is associated with different types of global bifurcations. In some cases these bifurcations involve connections to “infinity”.

For $f = 0$, Eqs. (4) and (5) reduce to the truncated normal form equations for the Hopf bifurcation with *exact* $D_4 \times S^1$ symmetry. This system has the following special solutions [20]. The trivial state $z_+ = z_- = 0$ always exists as an invariant set. Also, there are up to four types of nontrivial periodic solutions: u solutions with $z_+ = \pm z_-$, v solutions with $z_+ = \pm iz_-$, w solutions with $z_- = 0$ or $z_+ = 0$, and ns solutions with no nontrivial symmetry properties. Finally, quasiperiodic (hereafter qp) solutions may exist. The u, v, w solutions are *guaranteed* to bifurcate from the trivial state at $\lambda = 0$ by the Equivariant Branching Lemma, while the ns and qp solutions *may* bifurcate from the trivial state at $\lambda = 0$, depending on the values of A, B , and C . Where possible, we will interpret the solutions which are found for nonzero f in terms of the solutions which exist for $f = 0$.

To investigate possible connections to “infinity” when $f \neq 0$ we introduce the transformation [8]

$$z_+ = \rho^{-1/2} \cos(\frac{1}{2}\theta) e^{i(\phi+\psi)/2}, \quad z_- = \rho^{-1/2} \sin(\frac{1}{2}\theta) e^{i(-\phi+\psi)/2},$$

where, without loss of generality, $\theta \in [0, \pi]$, $\phi \in [-2\pi, 2\pi]$, and $\psi \in [0, 4\pi)$. In terms of the new time τ defined by $d\tau/dt = 1/\rho$, Eqs. (4) and (5) now take the form

$$\frac{d\rho}{d\tau} = -\rho[2A_R + B_R(1 + \cos^2\theta) + C_R \sin^2\theta \cos 2\phi] - 2[\lambda + f(\cos\phi \cos\psi - \cos\theta \sin\phi \sin\psi)]\rho^2, \quad (6)$$

$$\frac{d\theta}{d\tau} = \sin\theta[\cos\theta(-B_R + C_R \cos 2\phi) - C_I \sin 2\phi] + 2f\rho \sin\phi \sin\psi \sin\theta, \quad (7)$$

$$\frac{d\phi}{d\tau} = \cos\theta(B_I - C_I \cos 2\phi) - C_R \sin 2\phi - 2f\rho \cos\psi \sin\phi, \quad (8)$$

$$\frac{d\psi}{d\tau} = 2A_I + B_I + C_I \cos 2\phi + C_R \sin 2\phi \cos\theta + 2\omega\rho - 2f\rho \cos\phi \sin\psi. \quad (9)$$

If $f = 0$ the variable ψ decouples from the other three, but for $f \neq 0$ the system is fully four-dimensional. In the following we use $r \equiv 1/\rho = |z_+|^2 + |z_-|^2$ to denote the amplitude of a solution. Eqs. (6)–(9) have an invariant subspace Σ at $\rho = 0$ (corresponding to infinite amplitude states) on which the dynamics are equivalent to those for the system with $f = 0$. Since ψ decouples the dynamics on this subspace are two-dimensional [20], and hence simple to analyze. We label the fixed points in Σ by analogy to the finite amplitude fixed points of the problem in the absence of forcing ($f = 0$). Thus u_∞ solutions have $\rho = 0$, $\cos\theta = 0$, $\cos 2\phi = 1$; v_∞ solutions have $\rho = 0$, $\cos\theta = 0$, $\cos 2\phi = -1$; and w_∞ solutions have $\rho = 0$, $\sin\theta = 0$. All of these solutions correspond to time-periodic infinite amplitude solutions of Eqs. (6)–(9), and are always present. Under appropriate conditions two additional special solutions may also be present in Σ . For the coefficients considered in this paper infinite amplitude quasiperiodic solutions qp_∞ (corresponding to a limit cycle in Σ) will be present, but ns_∞ solutions (corresponding to nonsymmetric fixed points in Σ) will be absent. Under these conditions Eqs. (4) and (5) may possess solutions in the form of *bursts* with a very large dynamic range. The mechanism responsible for the presence of such bursts was elucidated in [8] albeit in a somewhat different context. In particular, suppose that a trajectory starts at finite amplitude and follows the stable manifold of a state $\mathcal{B} \in \Sigma$ (either an infinite amplitude periodic or a quasiperiodic solution) that is *unstable* within Σ . Such a trajectory describes a solution whose amplitude diverges to infinity. The instability of \mathcal{B} within Σ is now responsible for kicking the trajectory towards another state $\mathcal{A} \in \Sigma$. If this state is unstable in the ρ direction the trajectory escapes from Σ towards finite amplitude, thereby forming a burst. If there are no other attractors, bursts may occur repeatedly. Such repeated bursts are associated with heteroclinic cycles involving the infinite amplitude states \mathcal{A} and \mathcal{B} . A heteroclinic cycle of this type will exist if the following conditions hold [8]:

- (i) In the perfect problem ($f = 0$) the finite amplitude analog of $\mathcal{A}(\mathcal{B})$ is supercritical (subcritical) with respect to the bifurcation parameter λ .
- (ii) There is a trajectory $\mathcal{B} \rightarrow \mathcal{A}$ in the subspace Σ .
- (iii) There is a trajectory $\mathcal{A} \rightarrow \mathcal{B}$ out of the subspace Σ for some value of λ ($\lambda > 0$).

When \mathcal{B} has a one-dimensional unstable manifold within Σ while \mathcal{A} is attracting within Σ the connection $\mathcal{B} \rightarrow \mathcal{A}$ in Σ is structurally stable with respect to changes in the coefficients A , B and C , and independent of the parameters λ , ω , and f . In this case the formation of a heteroclinic cycle involving infinite amplitude solutions is a codimension one phenomenon. Moehlis and Knobloch [8] classify all connections of the above type and show that despite their heteroclinic nature the duration of the resulting bursts in the original time t is in fact *finite*. Of course, these infinite amplitude solutions are of physical interest only insofar as they are responsible for the presence of nearby solutions of large but finite amplitude, as discussed in [8].

3. A numerical example

In [8], we classified all possible connections to infinity of the above type, and the regions in coefficient space in which these may occur. However, whether these connections are in fact present can only be shown numerically

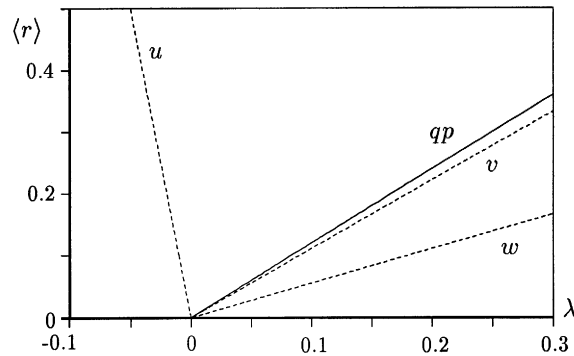


Fig. 1. Bifurcation diagram in the absence of forcing ($f = 0$) for $A = 1 - 1.5i$, $B = -2.8 + 5i$, $C = 1 + i$ and $\omega = 1$. Solid (broken) lines indicate stable (unstable) branches.

by determining the value(s) of λ at which the connection $\mathcal{A} \rightarrow \mathcal{B}$ forms. Below we present detailed results for the coefficient values

$$A = 1 - 1.5i, \quad B = -2.8 + 5i, \quad C = 1 + i, \quad \omega = 1,$$

and illustrate the type of complex behavior that results. For these coefficient values conditions (i) and (ii) are satisfied. Moreover, the connection involves the quasiperiodic solution at infinity and is therefore of particular interest. In Example 1(a) of [8], we show that the remaining condition (3) required for the formation of the connection holds for appropriate λ values once the $D_4 \times S^1$ symmetry is broken down to $D_2 \times S^1$; moreover, these coefficient values were used originally in [7] to suggest an explanation for the bursting behavior observed in experiments on binary fluid convection in large aspect ratio containers. We show below that similar behavior occurs when the S^1 symmetry is broken instead. In this paper, we do not consider the remaining possibilities identified in [8].

For these coefficient values and $f = 0$, the unstable u solutions bifurcate subcritically from the trivial state, while the unstable v and w solutions and the attracting quasiperiodic solutions qp all bifurcate supercritically [8]. Fig. 1 shows the resulting bifurcation diagram with λ as the bifurcation parameter and

$$\langle r \rangle \equiv \lim_{T \rightarrow \infty} \frac{1}{T} \int_0^T r(t) dt$$

as a measure of the amplitude. Moreover, the conditions for the formation of a heteroclinic connection to infinity listed in Section 2 are satisfied, with u_∞ and qp_∞ playing the role of the special solutions \mathcal{B} and \mathcal{A} , respectively. Indeed, Example 1(a) of [8] demonstrates that such a connection does indeed form when the D_4 symmetry of the problem that is broken to D_2 . In this case, there is a trajectory that goes from finite amplitude toward a u_∞ solution, gets kicked toward a qp_∞ solution, and then returns to finite amplitude, thereby forming a burst; at specific values of λ the presence of heteroclinic cycles of the type $\mathcal{A} \rightarrow \mathcal{B} \rightarrow \mathcal{A}$, describing an infinite sequence of such bursts, can be demonstrated numerically. These form because the symmetry-breaking terms are responsible for opening up a gap in λ in which neither the trivial state nor any of the simple finite amplitude states is stable. We investigate below the complementary situation that arises when the D_4 symmetry is retained but S^1 is broken instead, and show that an analogous gap opens up in this case as well. In the following, we fix $\lambda = 0.1$. In the absence of forcing, the special finite amplitude solutions which then exist are the unstable trivial state, the unstable, periodic w and v solutions, and the attracting, quasiperiodic qp solutions. Infinite amplitude u_∞ , v_∞ , w_∞ , and qp_∞ solutions are also present. Other choices of coefficients A , B , C , λ and ω yield similar bursting behavior, provided only that the conditions (i)–(iii), including the structural stability within Σ , continue to hold. In each

case the presence of forcing ($f \neq 0$) opens up an interval in λ in which neither the trivial state nor the finite amplitude qp state is stable; it is in these gaps that repeated bursts may be observed. We study the resulting equations using a combination of direct numerical integration in time, the program AUTO [21] for following unstable solution branches and their bifurcations, and the construction of appropriate return maps as necessary [8].

3.1. The supergluing bifurcation

Eqs. (4) and (5) contain four invariant subspaces ($z_- = 0$; $z_+ = 0$; $z_+ = z_-$; $z_+ = -z_-$) on which the dynamics are governed by an equation of the form

$$\dot{z} = (\lambda + i\omega)z + (a + ib)|z|^2z + f\bar{z}, \quad z \in \mathbb{C}. \tag{10}$$

This equation arises in the study of the perturbation of a standard Hopf bifurcation by resonant temporal forcing at (approximately) twice the Hopf frequency, and its dynamics are well understood [9,13,22]. Much of the behavior of Eq. (10) is governed by Takens–Bogdanov bifurcations, both with and without Z_2 symmetry (cf. [23]), and this fact provides a key to understanding the behavior of the system (4) and (5).

In the absence of forcing ($f = 0$) the system (4) and (5) possesses two distinct periodic w solutions, one of which lies in the invariant subspace $z_- = 0$ and the other in the invariant subspace $z_+ = 0$. In the presence of forcing ($f \neq 0$) these subspaces remain invariant and analogs of the w solutions continue, therefore, to exist. However, the interpretation of these solutions is now different: fixed points (FP_w) represent solutions that are phased-locked to the drive, while limit cycles (hereafter also referred to as w) correspond to quasiperiodic solutions. Fig. 2 shows a bifurcation diagram and sketches of the representative phase portraits for the dynamics restricted to these subspaces; stability is indicated only for perturbations within the subspaces. For our choice of coefficients only two special solutions are present in the interval $0 \leq f < \sqrt{\lambda^2 + \omega^2} = 1.00499$: the (unstable) trivial state and the (stable) analog of the w solution. At $f = 1.00499$ the trivial state undergoes a pitchfork bifurcation which gives birth to two new unstable fixed points labeled FP_w . The FP_w fixed points undergo a Hopf bifurcation at $f = 1.09835$ producing two symmetry-related unstable periodic orbits labeled P . These periodic orbits deform as f is increased to produce, via a gluing bifurcation SG, a pair of orbits homoclinic to the trivial state at $f = 1.12225$; for $f \gtrsim 1.12225$ the P periodic orbits no longer exist but a new unstable periodic orbit w' does. For reference, at the bifurcation SG the eigenvalues of the origin with eigenvectors within the two-dimensional subspace are 0.609 and -0.409 . The sum of these eigenvalues is $2\lambda = 0.2 > 0$, so the periodic orbits which participate in the bifurcation SG are expected to be (locally) unstable to perturbations within the invariant subspace (cf. [23]). The periodic orbits w and w' are annihilated in a saddle–node bifurcation at $f = 1.12968$, and for larger f only the (stable) FP_w solutions and (unstable) trivial state exist. Similar bifurcation diagrams arise in a number of other problems; in particular, for the time-reversed version of Fig. 2, see [24,25].

At the bifurcation SG, the connections to the trivial state occur in *both* subspaces $z_+ = 0$ and $z_- = 0$ simultaneously. However, as shown in the Appendix, there are generically no such connections in the invariant subspaces $z_+ = \pm z_-$ (for the coefficient values considered here). The bifurcation that results is a generalization of the gluing bifurcation and generates dynamics that are richer than would be expected from two independent gluing bifurcations; consequently we refer to this bifurcation as a *supergluing* bifurcation. The associated dynamics have already been described in the context of the Takens–Bogdanov bifurcation with D_4 symmetry in a limit in which the resulting equations are nearly $O(2)$ -symmetric [25]. In our example the supergluing bifurcation occurs at $(\lambda, \omega, f) = (0.1, 1, 1.12225)$, i.e., close to the codimension-two point $\lambda = 0, \omega = f$ for which Eqs. (4) and (5) have a Takens–Bogdanov bifurcation with D_4 symmetry; however, the values of the coefficients A, B , and C we use are far from the $O(2)$ -symmetric limit, and the analysis therefore differs (see Appendix). Some progress has

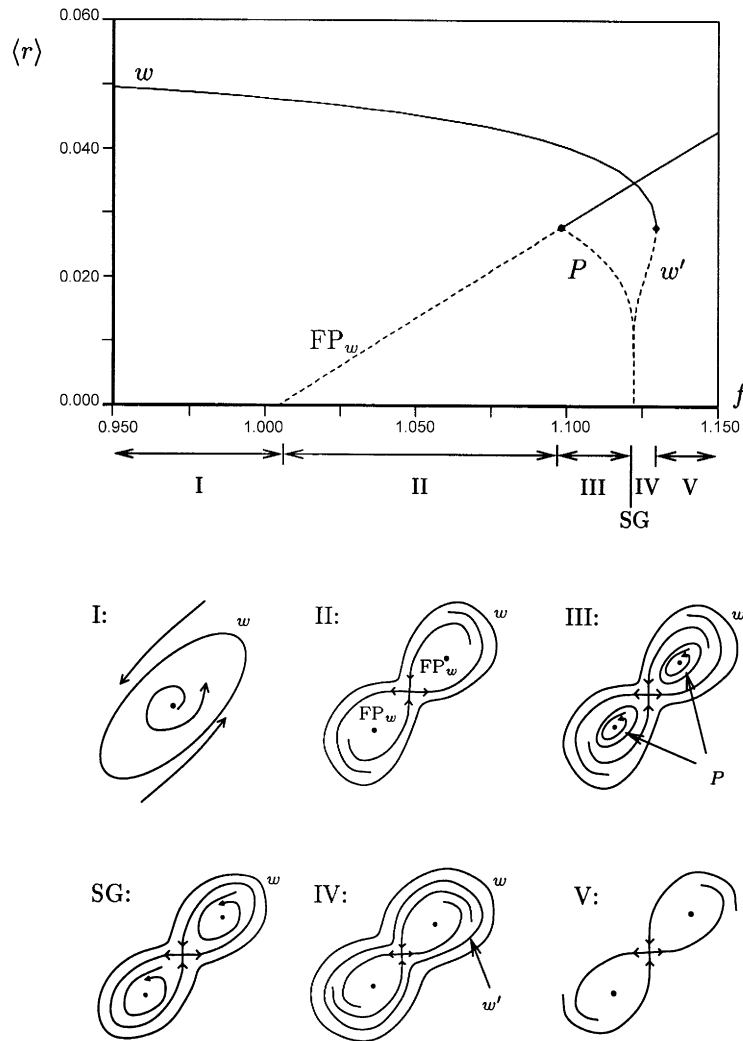


Fig. 2. Bifurcation diagram and sketches of phase portraits for the dynamics in the two-dimensional invariant subspaces $z_+ = 0$ and $z_- = 0$. In the bifurcation diagram, solid (broken) lines indicate stable (unstable) branches, where stability refers only to perturbations within the invariant subspace. As SG is approached, the periodic orbits spend more and more time near the origin and $\langle r \rangle \rightarrow 0$.

recently been made on the symbolic dynamics of trajectories near a related bifurcation in the Takens–Bogdanov normal form with D_3 symmetry [26].

Fig. 3 shows the four distinct orbits involved in this supergluing bifurcation. The numbers labeling these orbits are used to label the solution branches computed for the full system (4) and (5), cf. [26]. For example, as the w solutions in the $z_- = 0$ subspace approach the connection with the trivial state the trajectory traces out orbit 1 then orbit 2, then 1 again, etc. We therefore label this branch 12. There is also a symmetry-related connection involving the w solution in the $z_+ = 0$ subspace; we label this branch 34. Such symmetry-related branches will not be indicated in what follows. Similarly, there are four symmetry-related P solutions but the corresponding solution branch is labeled as 1.

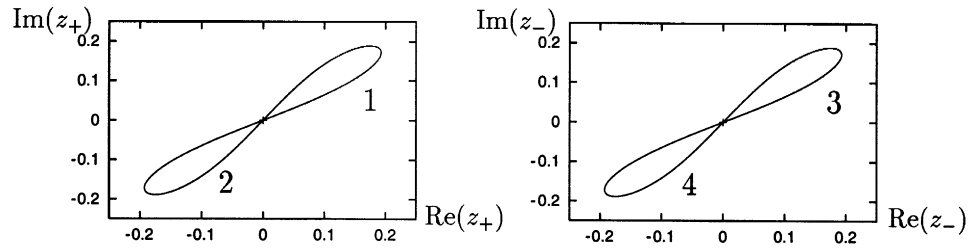


Fig. 3. At the supergluing bifurcation at $f = 1.12225$ there are four symmetry-related orbits forming homoclinic connections to the trivial state. Orbits 1 and 2 lie in the invariant subspace $z_- = 0$ while orbits 3 and 4 lie in the invariant subspace $z_+ = 0$.

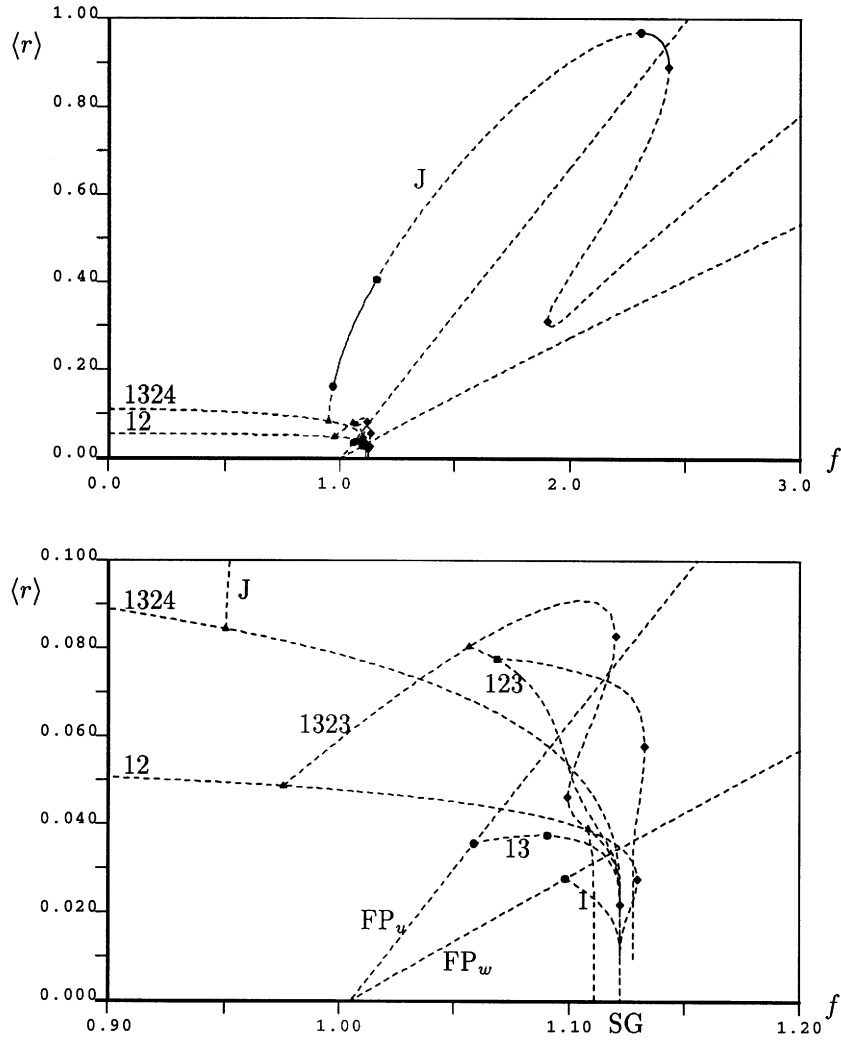


Fig. 4. Bifurcation diagrams showing the effect of forcing on the v (labeled 1324) and w (labeled 12) periodic solutions. Other related solutions are also shown. The lower diagram is a blow-up of the upper diagram, and circles, diamonds, squares, and triangles indicate Hopf, saddle–node, period-doubling, and symmetry-breaking pitchfork bifurcations, respectively. The supergluing bifurcation occurs at the point SG. See text for more details.

Fig. 4 shows the bifurcation diagram computed for the system (4) and (5) using the above labeling scheme. The diagram includes the results shown in Fig. 2, but shows stability properties with respect to *all* possible perturbations instead of just those in the appropriate invariant subspace. Observe that the analog of the w solution (labeled 12 in Fig. 4) is now always unstable, and that a new branch (labeled 1323; see Fig. 5(a)) whose solutions do not lie in one of the invariant subspaces $z_{\pm} = 0$ bifurcates off this branch at $f = 0.97592$. Successive bifurcations from this branch include the 123 branch (see Fig. 5(b)) and branches whose solutions are followed to the subsidiary global bifurcations at $f = 1.110772$ and 1.127792 . The period-doubling bifurcation from the 123 branch may be the beginning of a period-doubling cascade (see [25]), but the resulting chaos is apparently not attracting.

We now consider the analogs of the periodic v solutions. For $f = 0$ the v solutions lie in the invariant subspaces $z_+ = iz_-$ and $z_+ = -iz_-$; however, in the presence of forcing these subspaces are no longer invariant. This is because the isotropy subgroup of the v solutions involves an element of the normal form symmetry (cf. [27]), and this symmetry is broken by the temporal forcing. Fig. 4 shows that the branch of the corresponding periodic solutions is connected to the supergluing bifurcation SG, and that it consists of orbits of type 1324 (see Fig. 5(c)). Before reaching SG, however, there is a further bifurcation off this branch, at $f = 0.95059$, to a new branch of periodic solutions labeled J that are *stable* in the intervals $0.97019 < f < 1.15898$ and $2.30718 < f < 2.42837$; we will encounter the J solution several times in Section 3.2.

Finally, at $f = \sqrt{\lambda^2 + \omega^2} = 1.00499$ another type of fixed point solutions bifurcates from the trivial state [14], in addition to the FP_w fixed points already discussed. These lie in the invariant subspaces $z_+ = \pm z_-$ and

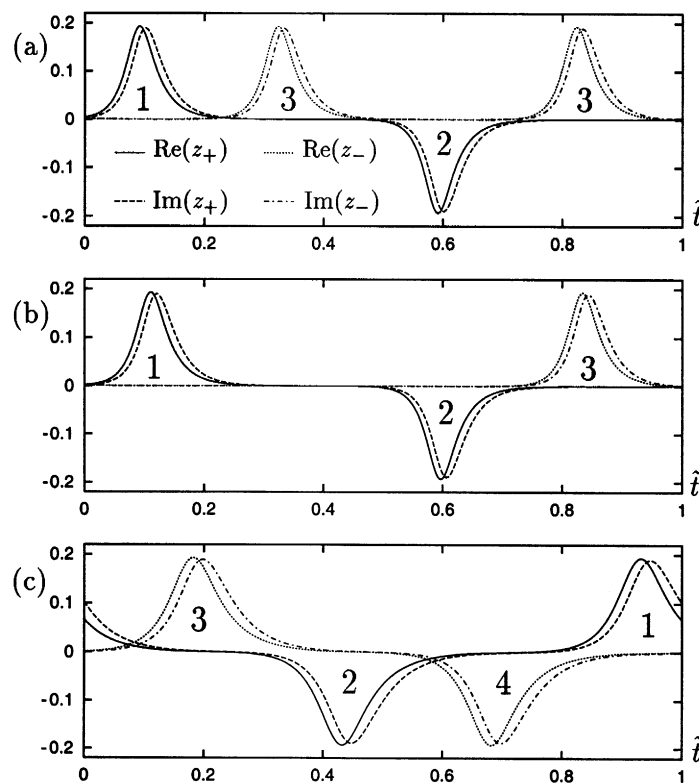


Fig. 5. Time series for the (a) 1323, (b) 123, (c) 1324 periodic orbits near the supergluing bifurcation SG obtained by following the orbits numerically to high period (normalized to unity). These periodic orbits are unstable. The numbers in the time series show which approximate homoclinic connection the trajectory is tracing out, labeled as in Fig. 3.

are labeled FP_u . These subspaces remain invariant even when $f \neq 0$. The corresponding fixed points undergo a Hopf bifurcation producing periodic solutions which remain in the corresponding invariant subspace and are also connected to the supergluing bifurcation SG; we label this branch 13. The 13 solutions themselves undergo a torus bifurcation at $f = 1.09051$ producing an *unstable* quasiperiodic solution. It is likely that this quasiperiodic solution undergoes the same type of wrinkling transition as described in Section 3.2. A number of features of Fig. 4 can be understood by analyzing the vicinity of the bifurcation SG as discussed further in the Appendix.

3.2. Attractors: wrinkled tori and bursts

Fig. 6 shows the attracting quasiperiodic solution which exists in the absence of forcing ($f = 0$) and for $f = 0.5$. As f increases further, this quasiperiodic solution deforms as it is “dragged” toward the u_∞ solutions (see Fig. 7); notice that the time series for $f = 0.98$ and 0.995 show burst-like behavior whenever the trajectory comes near the u_∞ solutions, but that the dynamic range of these bursts remains finite, i.e., the trajectories do not come arbitrarily

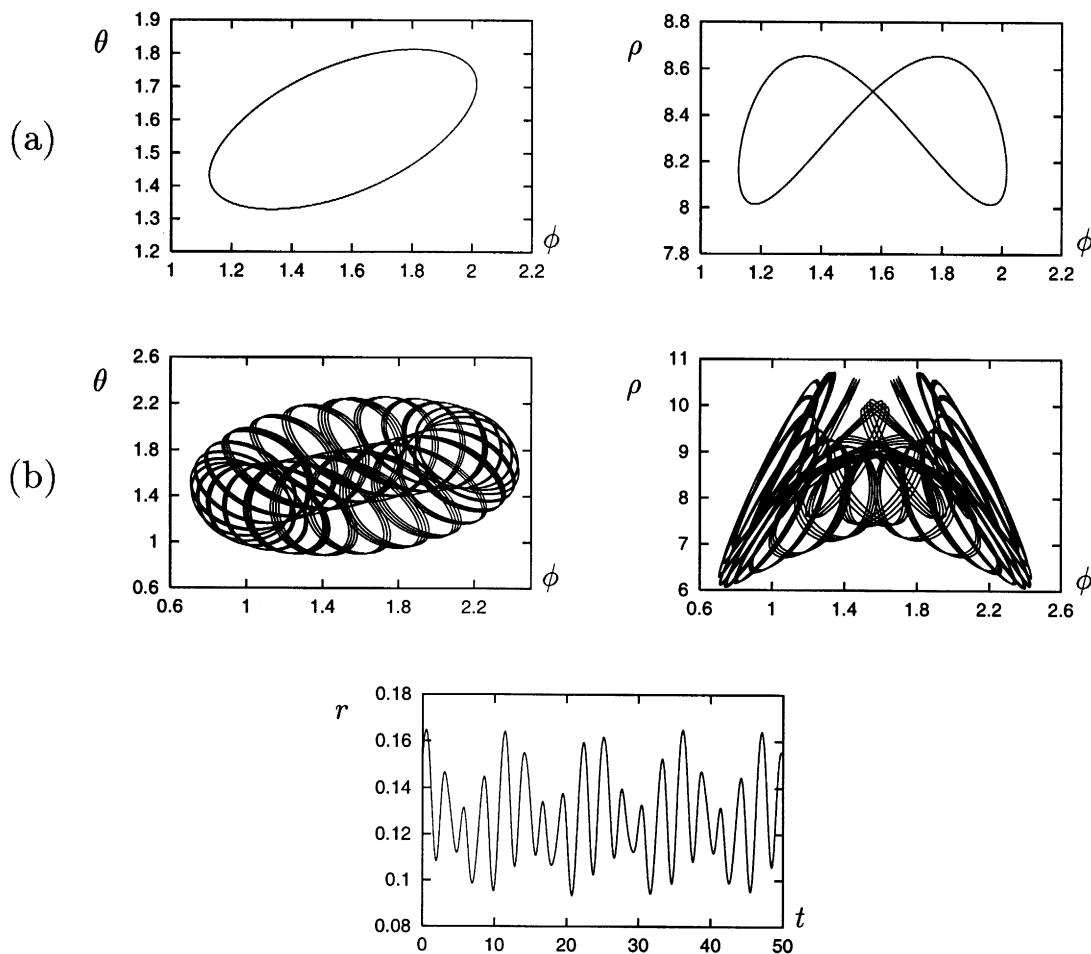


Fig. 6. Quasiperiodic solutions for (a) $f = 0$ and (b) $f = 0.5$. The solution shown in (a) appears periodic, but there is another frequency associated with the decoupled variable ψ .

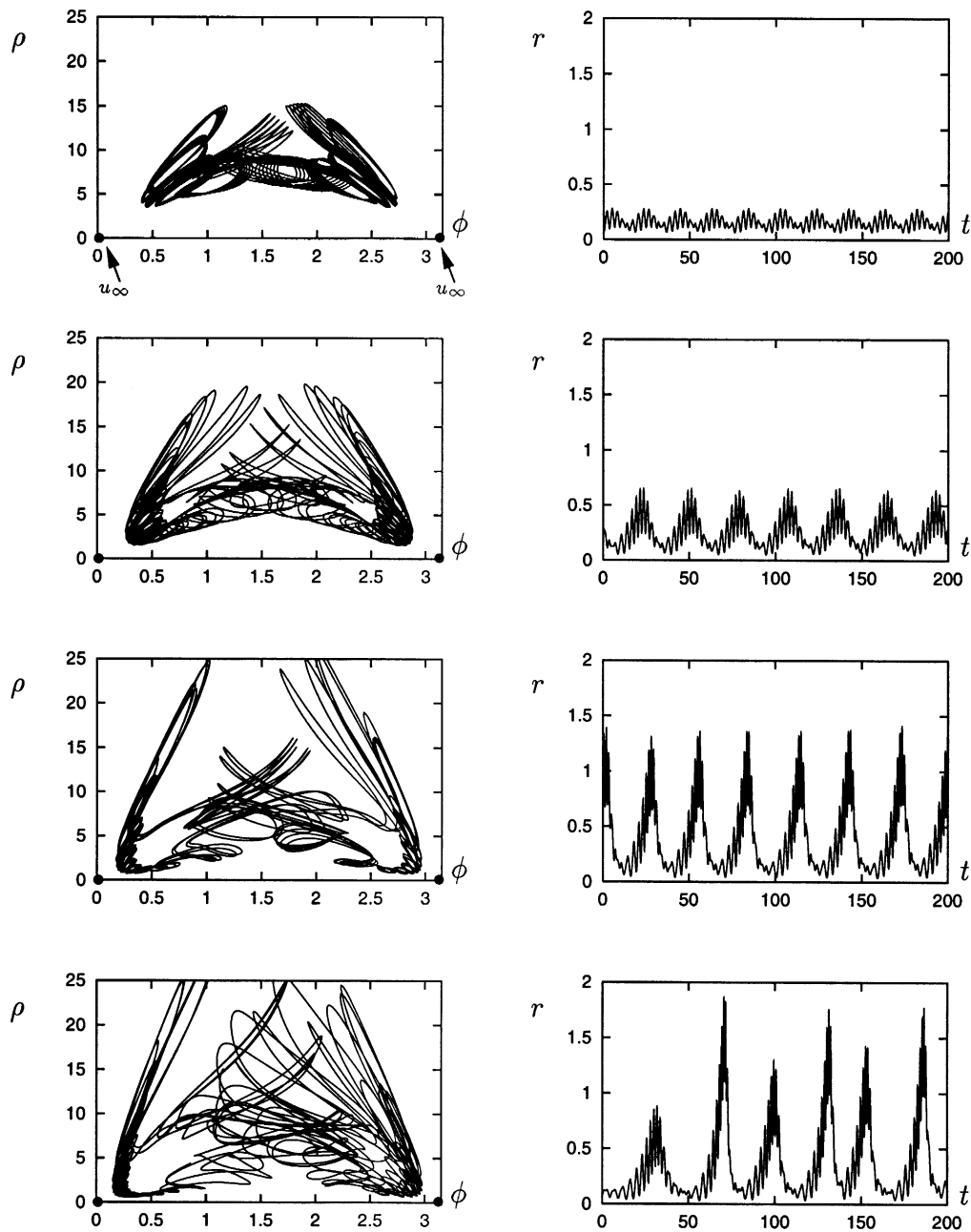


Fig. 7. Attracting solutions for (a) $f = 0.8$, (b) $f = 0.91$, (c) $f = 0.98$, and (d) $f = 0.995$. As f increases, the attractors are being “dragged” toward the u_∞ solutions denoted by the solid dots.

close to the plane $\rho = 0$. As f is increased over this range, there are also windows for which periodic solutions exist; examples of such solutions are shown in Fig. 8.

A useful way to represent this change in the attractor is to consider Poincaré maps constructed by intersecting the flow with a hyperplane defined by $\psi = \text{constant}$. If such a map traces out a circle, the corresponding solution

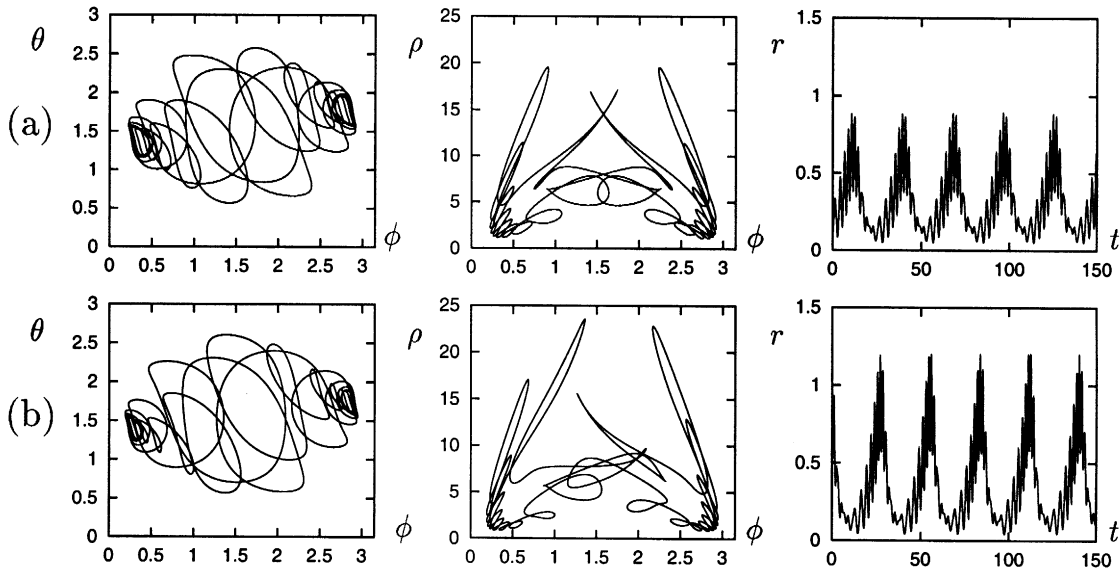


Fig. 8. Stable periodic solutions for (a) $f = 0.94$ and (b) $f = 0.968$. Notice that different periodic solutions may have different symmetry properties.

to the full equations lies on a torus and is quasiperiodic; on the other hand, if such a map traces out a discrete set of points the corresponding solution to the full equations is periodic. Poincaré maps for different values of f are shown in Fig. 9. Evidently as f increases the invariant circle develops wrinkles and eventually breaks down, producing chaotic behavior. There are also windows in f with stable periodic solutions. Such a transition from a quasiperiodic solution to chaos with periodic windows has been observed experimentally [28–31], in numerical studies of ordinary differential equations [32,33], as well as in two-dimensional invertible maps [34–37]. The discussion of [35,36] is particularly useful for qualitatively understanding the transition. Here the delayed logistic map, which contains an invariant circle for a range of parameters, is embedded in a two-parameter family of maps containing a hyperbolic fixed point at the origin. As a parameter is varied and the invariant circle grows towards the origin, periodic solutions are born in saddle–node bifurcations when an Arnol’d tongue is entered and destroyed again when the tongue is left. Inside each tongue these periodic solutions may be labeled by their rotation number. We define Θ to be the angular coordinate on the invariant circle. The rotation number for a periodic orbit is then

$$R \equiv \frac{1}{2\pi} \lim_{m \rightarrow \infty} \frac{1}{m} \sum_{n=0}^{m-1} (\Theta_{n+1} - \Theta_n),$$

where Θ_n is the Θ value for the n th iteration of the Poincaré map. The rotation number thus measures the “average fraction” around the invariant circle that the solution moves under each iteration of the Poincaré map. It is conjectured in [35,36] that by varying a single system parameter there is an infinite number of intervals for which only periodic orbits with a unique rotation number exist, and that these are interspersed among an infinite number of intervals for which periodic orbits with different rotation numbers coexist. The details of the periodic windows are thus expected to be very complicated. It is also demonstrated in [35,36] that far from the tip of the Arnol’d tongue, the invariant circle becomes wrinkled due to tangencies of invariant manifolds of the periodic orbits which arise at the saddle–node bifurcations at the edge of a tongue, producing chaotic behavior inside the tongue (via associated period-doubling cascades). Overall, the behavior of the system is governed by the approach as parameters are varied

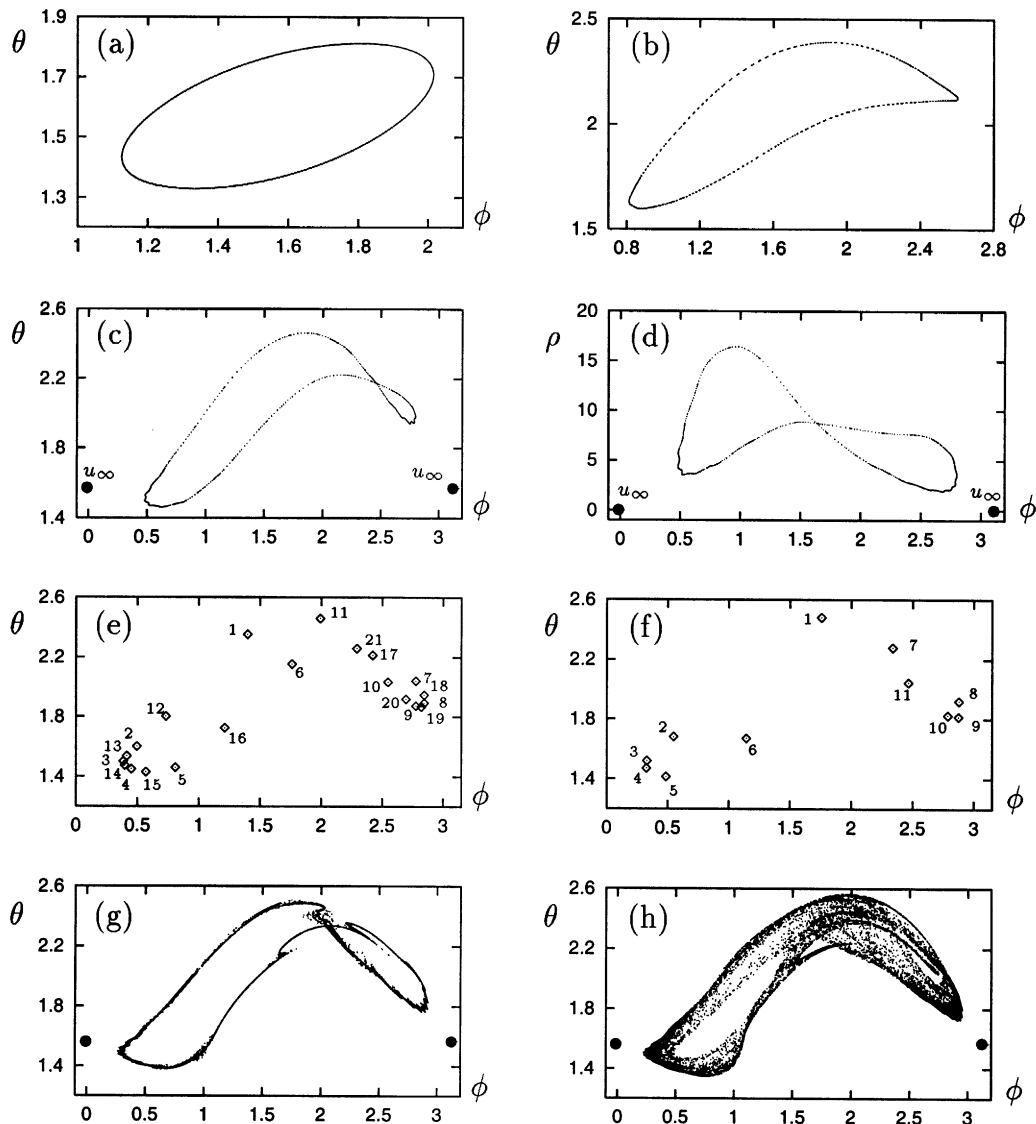


Fig. 9. Poincaré maps constructed by intersecting the flow with the hyperplane $\psi = 10$ (from smaller to larger values) for (a) $f = 0$, (b) $f = 0.8$, (c,d) $f = 0.91$, (e) $f = 0.94$, (f) $f = 0.968$, (g) $f = 0.98$, (h) $f = 0.995$. Figures (c,d) show the wrinkling associated with proximity to the u_∞ solutions. The integers in (e) and (f) label the successive locations at which the flow pierces the hyperplane; the rotation numbers for these periodic orbits are thus (e) $2/21$ and (f) $1/11$. In (g) and (h) the torus has been destroyed, and the system behaves chaotically. Note that the apparent self-intersections of the attractors are an artifact of the projection which has been chosen for the display.

of the invariant circle to the stable manifold of an unstable fixed point of the system, although the invariant circle disappears much before such a homoclinic connection can take place. These predictions, admittedly derived from studies of model systems, fit well with what is observed in the present problem: the wrinkling of the torus into chaos and the formation of periodic windows appear to be governed by the approach of the attractor to the periodic u_∞ solutions as f increases. Moreover, the observed chaotic dynamics appear to be associated with connections other than those involving solutions in the Σ subspace. In fact the attractor is destroyed still at finite amplitude by a

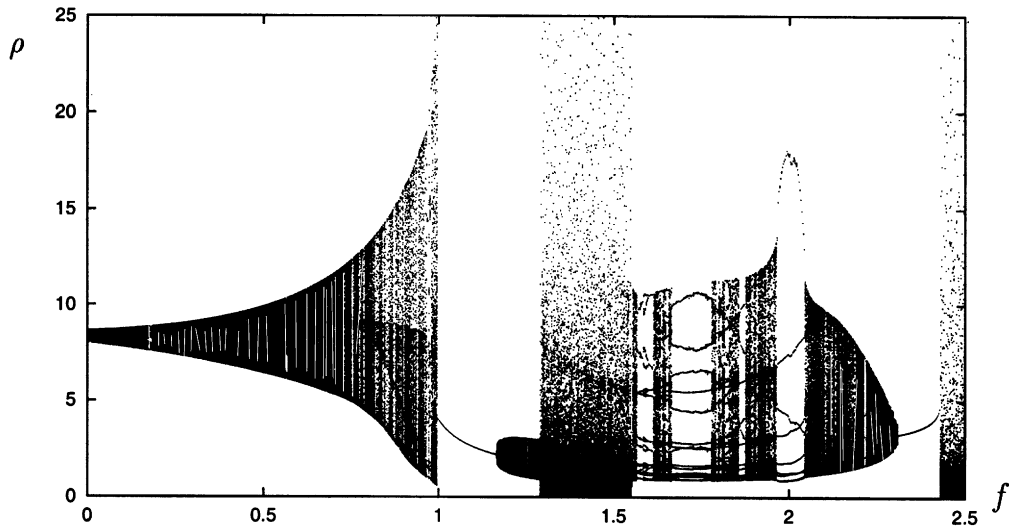


Fig. 10. Bifurcation diagram showing the instantaneous value of ρ whenever the trajectory pierces the Poincaré section defined by $\psi = 10$ (from smaller to larger values) after the transients have died out. The plot is generated by adiabatically increasing the value of f from $f = 0$, omitting transients. Coexisting attractors (including symmetry-related attractors) are therefore absent.

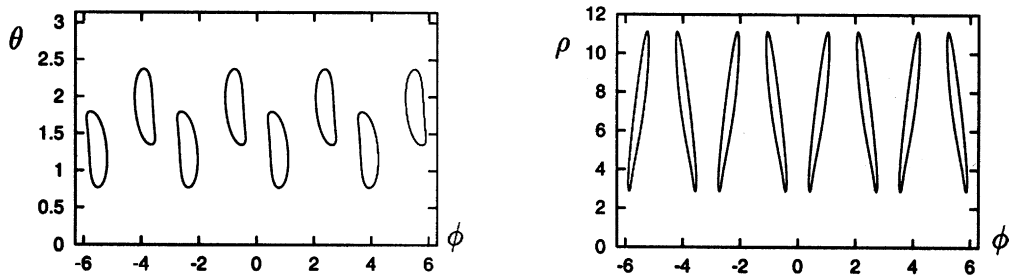


Fig. 11. Stable symmetry-related periodic J solutions for $f = 1$.

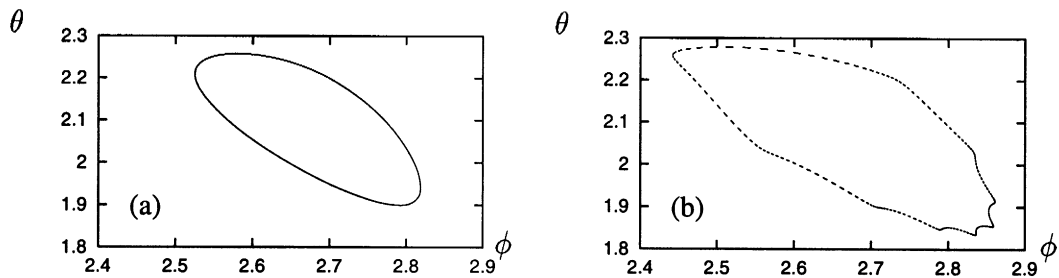


Fig. 12. Poincaré maps constructed by intersecting the flow with the hyperplane $\psi = 10$, showing (a) an attracting quasiperiodic solution on a torus when $f = 1.2$, and (b) a wrinkled torus when $f = 1.28$.

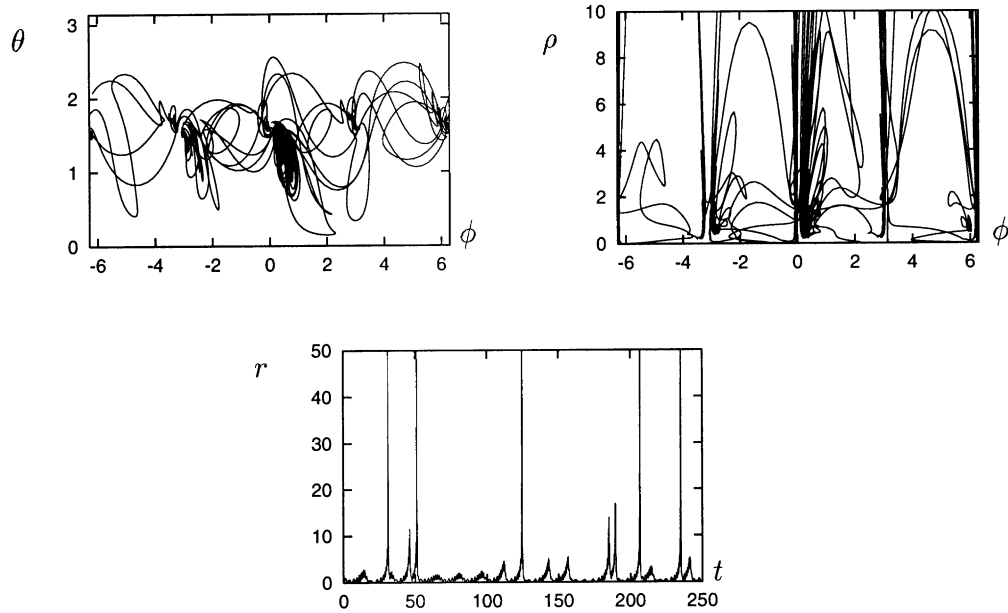


Fig. 13. Attractor for $f = 1.5$ showing bursts arising from repeated visits near the u_∞ solutions at $(\rho, \theta, \phi) = (0, \frac{1}{2}\pi, m\pi)$, where $m = -2, -1, 0, 1, 2$. The dynamic range of the bursts is very large, and bursts with arbitrarily large r may occur.

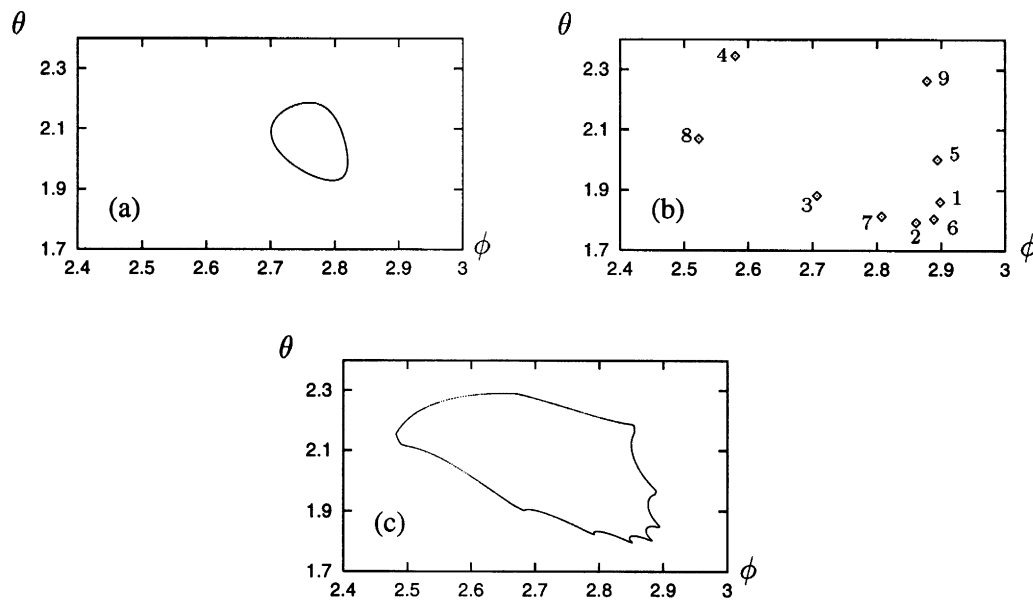


Fig. 14. Poincaré maps constructed by intersecting the flow with the hyperplane $\psi = 10$ for (a) $f = 2.25$, showing an attracting quasiperiodic solution on a torus, (b) $f = 2$, showing a stable periodic orbit, and (c) $f = 1.9$, showing how the torus has become wrinkled. The numbers in (b) label the successive locations at which the flow pierces the hyperplane, and indicate that this periodic orbit has rotation number $2/9$.

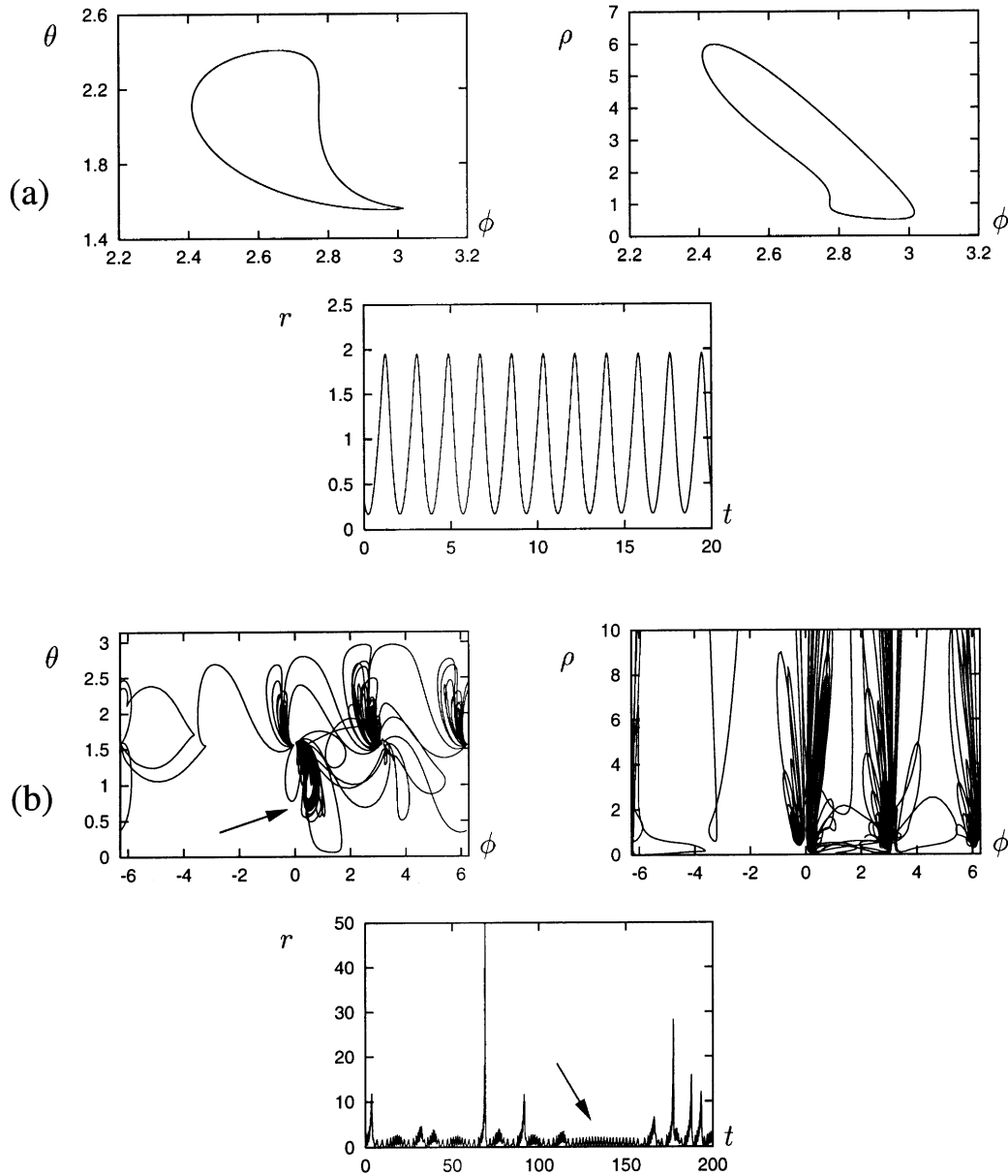


Fig. 15. Attractors for (a) $f = 2.4283$ and (b) $f = 2.4284$. The attractor in (a) is a stable J solution; such solutions cease to exist due to the saddle–node bifurcation at $f = 2.42837$. The time series in (b) exhibits bursts due to repeated visits near the u_∞ and qp_∞ solutions, and also makes occasional visits near the “ghost” of a J solution, indicated by the arrow. The onset of bursting as f increases through 2.42837 is via Type I intermittency.

boundary crisis at $f \approx 0.9975$ when it collides with the stable manifold of an unstable periodic orbit (cf. [38,39]). Fig. 10 shows the occurrence of this crisis and other important transitions in the attractor as f is varied.

For $f \gtrsim 0.9975$ the attractor is the finite amplitude J solution shown for $f = 1$ in Fig. 11. This solution itself loses stability in a torus bifurcation at $f = 1.15898$, producing a quasiperiodic solution which wrinkles with increasing

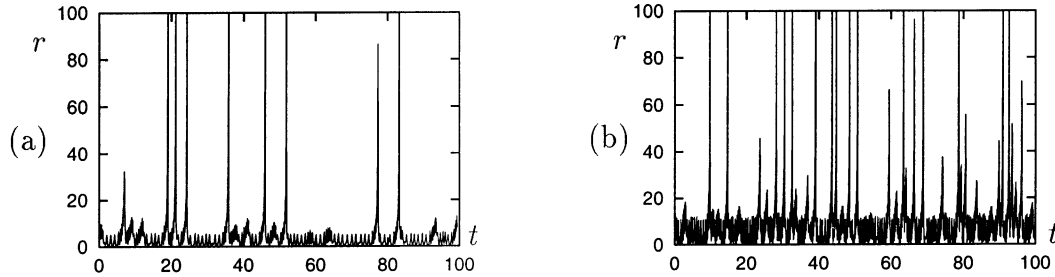


Fig. 16. Time series showing that bursts persist for (a) $f = 5$ and (b) $f = 10$.

f as shown in Fig. 12. At $f \approx 1.29$ the attractor is enlarged in an interior crisis (see Fig. 10) resulting in bursting behavior in which the trajectory makes visits very close to $\rho = 0$ (see Fig. 13). As in the situation described in [8], a burst occurs when the trajectory makes a visit near a u_∞ solution, traverses toward a qp_∞ solution, before returning to small amplitude. Such bursts, first found in a model for large aspect-ratio binary fluid convection [6,7], have unlimited dynamic range in contrast with most other burst mechanisms which have been studied [40,41].

The J solution is also stable in the interval $2.30718 \lesssim f \lesssim 2.42837$; as f decreases below $f \approx 2.30718$, the J solution undergoes a torus bifurcation and the resulting attractor wrinkles into chaos interspersed with periodic windows (see Figs. 10 and 14). The onset of bursting that occurs as f decreases through $f \approx 1.55$ is due to an interior crisis. In contrast, as f increases through $f \approx 2.42837$ the J solution is destroyed in a saddle–node bifurcation (see Fig. 4), with bursts occurring for values of f beyond this bifurcation (see Figs. 10 and 15), i.e., here bursts set in via Type I intermittency [42]. However, in the present system the change in the dynamic range in passing through the saddle–node bifurcation is very large (in principle, infinite). Fig. 16 shows that the resulting bursts persist to larger values of f .

4. Conclusion

In this paper we have explored the possibility that parametric forcing might have a similar effect on the Hopf bifurcation with D_4 symmetry as breaking of the D_4 symmetry down to D_2 . In the latter case we have discovered [6–8] that even small symmetry-breaking could have a dramatic effect because it opens up an interval of parameter values in which all the simple states of the system are unstable. The appearance of complex dynamics in such an interval is therefore inevitable. However, in contrast to related work by Hirschberg and Knobloch [5] on breaking $O(2)$ down to D_2 , in the D_4 -symmetric case the dynamics took the form of regular or irregular bursts of very large dynamic range. The occurrence of these bursts can be attributed to the presence for nearby parameter values of a heteroclinic connection to “infinity” [7,8]. In the present paper, we have shown that parametric forcing has a similar effect, and focused attention on the resulting dynamics in what we consider to be the most interesting regime, namely one involving the infinite amplitude unstable quasiperiodic states. As a result, the behavior we described not only involved similar connections to “infinity” but was in addition complicated by the destruction of an invariant torus due to the formation of these connections. It is the combination of these two dynamical phenomena that appears to be responsible for the complexity of the results we have described.

In the example explored in this paper certain aspects of the observed dynamical behavior can be related to the appearance in the system of a new type of global bifurcation involving the origin. This bifurcation (which we call a “supergluing bifurcation”) is introduced by the parametric forcing, and organizes the u , v and w periodic orbits, as well as others that are introduced by the forcing. This fact helps us connect the analysis of the Hopf bifurcation with D_4 symmetry in the *absence* of forcing [20] with the local bifurcation analysis of fixed points in the *presence* of

forcing [14]. In contrast the complex transitions associated with the wrinkling of the torus with increasing forcing can be attributed to the approach of the resulting attractor to the u_∞ solutions. In this regime various parameter windows are present in which stable periodic solutions are found, and these are associated with the traversal in parameter space through Arnol'd tongues. However, the resulting attractor does not reach the u_∞ solutions because it is destroyed in a boundary crisis. Despite this, there are *other* ranges of f for which the attractor does apparently come arbitrarily close to the u_∞ solutions, forming a sequence of irregular bursts of *infinite* dynamic range (see Fig. 10). In the particular example discussed here this type of bursting can appear either via an interior crisis or via Type I intermittency.

Reasoning similar to that given in [8] suggests that this type of bursting behavior can persist even when higher terms in Eqs. (4) and (5) are retained. Bursts will then be associated with visits near large but *finite* amplitude solutions. Thus bursts similar to those described in this paper may be observed in real physical systems undergoing a Hopf bifurcation with D_4 symmetry, such as overstable systems in domains of square cross-section and spring-supported fluid-conveying tubes with pulsatile flow [43,44]. In other systems, such as the Faraday system in a square container [45–49], there is no instability in the absence of forcing and all infinitesimal disturbances decay ($\lambda < 0$). As discussed in [7,8] the key requirement for bursting is the presence of a trajectory between two infinite amplitude solutions, $\mathcal{B} \rightarrow \mathcal{A}$ in the plane Σ , in circumstances in which (in the absence of forcing) the finite amplitude analogs of $\mathcal{A}(\mathcal{B})$ are supercritical (subcritical). Under these circumstances a suitable breaking of the $D_4 \times S^1$ symmetry of the unperturbed problem (either by breaking the D_4 symmetry or by temporal forcing, which breaks the S^1 symmetry) may produce a finite amplitude connection $\mathcal{A} \rightarrow \mathcal{B}$ so that repeated bursts will occur whenever a trajectory starts near the stable manifold of \mathcal{B} . Note, however, that in systems like the Faraday system we do not expect the presence of any subcritical branches in the absence of forcing; such branches can only appear as a result of the forcing itself, but once present these could produce bursts by the above mechanism as well.

Acknowledgements

This work was supported by NASA under grant NAG3-2152. JM also acknowledges the support of a National Science Foundation Mathematical Sciences Postdoctoral Research Fellowship. We thank J. Porter and A. Rucklidge for helpful discussions.

Appendix A. The supergluing bifurcation

A.1. Existence of the bifurcation

Eqs. (4) and (5) restricted to the invariant subspaces $z_+ = 0$ or $z_- = 0$ take the form

$$\dot{y} = (\lambda + i\omega)y + f\bar{y} + (A + B)|y|^2y, \quad y \in \mathbb{C}. \quad (\text{A.1})$$

Thus, if a gluing bifurcation involving the origin occurs in (A.1), it occurs simultaneously in *both* invariant subspaces $z_+ = 0$ and $z_- = 0$. Since such a gluing bifurcation is of codimension one, the supergluing bifurcation for Eqs. (4) and (5) is also of codimension one.

Eqs. (4) and (5) also have the invariant subspaces $z_+ = z_-$ and $z_+ = -z_-$ on which the dynamics are governed by the equation

$$\dot{z} = (\lambda + i\omega)z + f\bar{z} + (2A + B + C)|z|^2z, \quad z \in \mathbb{C}. \quad (\text{A.2})$$

If a gluing bifurcation involving the origin occurs in these equations, it again occurs in both invariant subspaces

simultaneously, and so is of codimension one. Such a bifurcation thus produces four connections to the origin $(0, 0)$ in the system (4) and (5).

With

$$\tilde{y} = \sqrt{A_R + B_R y}, \quad \tilde{z} = \sqrt{2A_R + B_R + C_R z},$$

Eqs. (A.1) and (A.2) become

$$\dot{\tilde{y}} = (\lambda + i\omega)\tilde{y} + f\bar{\tilde{y}} + \left(1 + i\frac{A_I + B_I}{A_R + B_R}\right)|\tilde{y}|^2\tilde{y}, \quad (\text{A.3})$$

$$\dot{\tilde{z}} = (\lambda + i\omega)\tilde{z} + f\bar{\tilde{z}} + \left(1 + i\frac{2A_I + B_I + C_I}{2A_R + B_R + C_R}\right)|\tilde{z}|^2\tilde{z}, \quad (\text{A.4})$$

where $A = A_R + iA_I$, etc. Eqs. (A.3) and (A.4) are *identical* when

$$(A_R + B_R)(2A_I + B_I + C_I) = (A_I + B_I)(2A_R + B_R + C_R).$$

Under this additional condition, a gluing bifurcation in one of the four invariant subspaces $z_+ = 0$, $z_- = 0$, $z_+ = z_-$, $z_+ = -z_-$ implies a gluing bifurcation in the other three, giving a total of eight connections to the origin. Note that the connections in the subspaces $z_+ = 0$ and $z_- = 0$ are “scaled” relative to the connections in the subspaces $z_+ = z_-$ and $z_+ = -z_-$. This bifurcation is evidently of codimension two. Finally, Eqs. (A.1) and (A.2) are made identical by choosing $A = -C$, giving eight *identical* connections to the origin. This is a codimension three bifurcation because it requires $A_R = -C_R$ and $A_I = -C_I$, and one more parameter (such as f) needs to be varied in order to reach it.

It is natural to ask if related bifurcations can occur in the resonantly forced Hopf bifurcation with $O(2)$ symmetry. If the Hopf frequency is ω_0 and the external forcing frequency is $\omega_e \approx n\omega_0$ for $n = 1, 2$, the normal form equations for this situation are [11,12]

$$\begin{aligned} \dot{z}_1 &= (\lambda + i\omega)z_1 + f\bar{z}_2 + A(|z_1|^2 + |z_2|^2)z_1 + B|z_1|^2z_1, \\ \dot{z}_2 &= (\lambda + i\omega)z_2 + f\bar{z}_1 + A(|z_1|^2 + |z_2|^2)z_2 + B|z_2|^2z_2, \end{aligned}$$

where $(z_1, z_2) \in \mathbb{C}^2$, f is the (real) strength of the forcing, and $\omega \equiv \omega_0 - \omega_e/n$ is again the detuning. In contrast to (4) and (5) these equations have a *circle* of invariant subspaces $(z_1, z_2) = (e^{-i\sigma}z, e^{i\sigma}z)$, where $z \in \mathbb{C}$ and $\sigma \in [0, 2\pi)$, on which the dynamics are governed by the equation

$$\dot{z} = (\lambda + i\omega)z + f\bar{z} + (2A + B)|z|^2z. \quad (\text{A.5})$$

Thus, if a gluing bifurcation occurs in Eq. (A.5), it occurs simultaneously in each of the invariant subspaces that make up the circle of invariant subspaces, and there is then an (uncountably) infinite number of distinct (but symmetry-related) homoclinic connections to the origin. This is in contrast to the supergluing bifurcation in the resonantly forced Hopf bifurcation with D_4 symmetry in which gluing bifurcations occur in a *finite* number of invariant subspaces. In the latter case the associated dynamics are described very well by a one-dimensional map [25], provided the equations are nearly $O(2)$ -symmetric (i.e., $0 < |C| \ll 1$); unfortunately this is not the case for general values of C .

A.2. Analysis

To discuss the dynamics near the supergluing bifurcation we choose local coordinates such that the linearized equations near the origin take the form

$$\dot{x}_1 = \lambda_u x_1 + \dots, \quad \dot{x}_2 = -\lambda_s x_2 + \dots, \quad \dot{x}_3 = \lambda_u x_3 + \dots, \quad \dot{x}_4 = -\lambda_s x_4 + \dots,$$

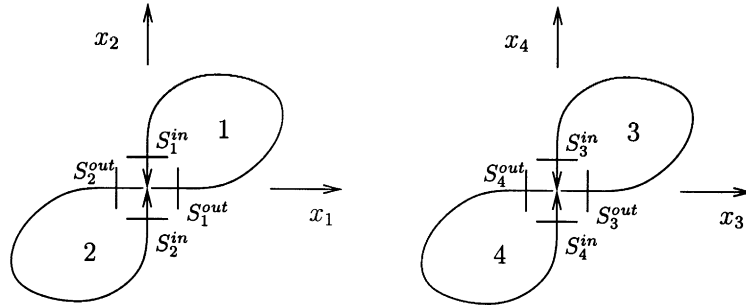


Fig. 17. Coordinates and surfaces of section for the analysis of the supergluing bifurcation. The four symmetry-related homoclinic connections to the origin present at $\mu = 0$ are labeled by integers as in the text.

where $\lambda_u, \lambda_s > 0$, and the dots denote nonlinear terms. Without loss of generality, we consider $\lambda_s < \lambda_u$; if this condition does not hold we reverse time and relabel the axes so that it does. We let μ be an unfolding parameter such that the four symmetry-related homoclinic orbits are present at $\mu = 0$ (see Fig. 17), but are broken when $\mu \neq 0$. We define the following surfaces of section (see Fig. 17):

$$\begin{aligned} S_1^{\text{in}} &= \{(x_1, x_2, x_3, x_4) | x_2 = c\}, & S_1^{\text{out}} &= \{(x_1, x_2, x_3, x_4) | x_1 = c\}, \\ S_2^{\text{in}} &= \{(x_1, x_2, x_3, x_4) | x_2 = -c\}, & S_2^{\text{out}} &= \{(x_1, x_2, x_3, x_4) | x_1 = -c\}, \\ S_3^{\text{in}} &= \{(x_1, x_2, x_3, x_4) | x_4 = c\}, & S_3^{\text{out}} &= \{(x_1, x_2, x_3, x_4) | x_3 = c\}, \\ S_4^{\text{in}} &= \{(x_1, x_2, x_3, x_4) | x_4 = -c\}, & S_4^{\text{out}} &= \{(x_1, x_2, x_3, x_4) | x_3 = -c\}, \end{aligned}$$

where $c > 0$ and is sufficiently small that the linearized equations apply in $|x_j| < c, j = 1, 2, 3, 4$.

We consider first the linear maps $P_{lm}^{\text{loc}} : S_l^{\text{in}} \rightarrow S_m^{\text{out}}$, focusing on $m = 1$ and $l = 1, 2, 3, 4$, noting that the remaining maps may be obtained by symmetry. Suppose that the trajectory intersects the surface of section S_l^{in} at $(x_{10}, x_{20}, x_{30}, x_{40})$ (one of these will be equal to $\pm c$ depending on the value of l). The time of flight from S_l^{in} to S_1^{out} follows from the condition $c = x_{10} e^{\lambda_u T}$ (which requires $x_{10} > 0$), i.e.,

$$T = \frac{1}{\lambda_u} \ln \left| \frac{c}{x_{10}} \right|.$$

Using this expression in the linearized equations for the flow near the origin,

$$P_{l1}^{\text{loc}} : (x_{10}, x_{20}, x_{30}, x_{40}) \rightarrow \left(c, \left| \frac{x_{10}}{c} \right|^\delta x_{20}, \left| \frac{c}{x_{10}} \right| x_{30}, \left| \frac{x_{10}}{c} \right|^\delta x_{40} \right),$$

where $\delta = \lambda_s / \lambda_u > 0$. Since we are considering without loss of generality $\lambda_s < \lambda_u$, we have $0 < \delta < 1$.

We consider next the global map $P_1^{\text{glo}} : S_1^{\text{out}} \rightarrow S_1^{\text{in}}$. An approximation to this map is found by expanding about the exact homoclinic orbit (labeled 1) which forms when $\mu = 0$. The linearization about this homoclinic orbit block-diagonalizes, with one block corresponding to behavior inside the $x_1 = x_2 = 0$ invariant subspace, and the other corresponding to behavior in the $x_3 = x_4 = 0$ invariant subspace. Thus,

$$P_1^{\text{glo}} : (c, x_2, x_3, x_4) \rightarrow (\gamma x_2 + \mu, c, \alpha_1 x_3 + \beta_1 x_4, \alpha_2 x_3 + \beta_2 x_4), \tag{A.6}$$

where $\gamma > 0$, $\alpha_1\beta_2 - \alpha_2\beta_1 \neq 0$ for invertibility, and hence

$$P_1^{\text{glo}} \circ P_{11}^{\text{loc}} : \begin{pmatrix} x_{10} \\ x_{20} \\ x_{30} \\ x_{40} \end{pmatrix} \rightarrow \begin{pmatrix} \gamma \left| \frac{x_{10}}{c} \right|^\delta x_{20} + \mu \\ c \\ \alpha_1 \left| \frac{c}{x_{10}} \right| x_{30} + \beta_1 \left| \frac{x_{10}}{c} \right|^\delta x_{40} \\ \alpha_2 \left| \frac{c}{x_{10}} \right| x_{30} + \beta_2 \left| \frac{x_{10}}{c} \right|^\delta x_{40} \end{pmatrix}. \quad (\text{A.7})$$

The maps $P_2^{\text{glo}} \circ P_{12}^{\text{loc}}$, $P_3^{\text{glo}} \circ P_{13}^{\text{loc}}$ and $P_4^{\text{glo}} \circ P_{14}^{\text{loc}}$ are related to this map by symmetry. By composing such maps appropriately, we may obtain three-dimensional maps from a surface of section into itself corresponding to a trajectory which follows any sequence of the homoclinic orbits 1, 2, 3, 4. Fixed points of such three-dimensional maps correspond to periodic orbits in the four-dimensional vector field.

We illustrate this procedure for four types of periodic orbits found numerically, namely those labeled 1, 12, 13, and 1324 (see Fig. 4), taking advantage of appropriate symmetry properties of the periodic orbits to simplify the analysis. To find periodic orbits of type 1, consider the fixed points of the map $P_1^{\text{glo}} \circ P_{11}^{\text{loc}} : S_1^{\text{in}} \rightarrow S_1^{\text{in}}$. Restricting to $x_3 = x_4 = 0$, Eq. (A.7) reduces to the one-dimensional map

$$x_{10} \rightarrow c\gamma \left| \frac{x_{10}}{c} \right|^\delta + \mu. \quad (\text{A.8})$$

This map is easily analyzed [23] and shows that when $\delta < 1$ a fixed point (i.e., a periodic orbit of type 1) exists only for $\mu < 0$.

Consider next the map $P_1^{\text{glo}} \circ P_{21}^{\text{loc}} : S_2^{\text{in}} \rightarrow S_1^{\text{in}}$. Restricting again to the $x_3 = x_4 = 0$ subspace, Eq. (A.7) reduces to the one-dimensional map

$$x_{10} \rightarrow -c\gamma \left| \frac{x_{10}}{c} \right|^\delta + \mu, \quad (\text{A.9})$$

with x_{20} mapped from $-c$ to c . We look for periodic orbits $(x_1^*(t), x_2^*(t))$ with period T and the symmetry property

$$(x_1^*(t + \frac{1}{2}T), x_2^*(t + \frac{1}{2}T)) = (-x_1^*(t), -x_2^*(t)). \quad (\text{A.10})$$

A map (A.9) that maps x_{10} to $-x_{10}$ corresponds to evolution in time by $\frac{1}{2}T$ starting in S_2^{in} and ending in S_1^{in} after time $\frac{1}{2}T$. A fixed point with this property corresponds to an orbit of period T and symmetry (A.10) in the four-dimensional system. Since during the first half of the period the trajectory follows homoclinic orbit 1, it will follow over the next $\frac{1}{2}T$ the homoclinic orbit labeled 2, i.e., fixed points of the equation

$$-x_{10} = -c\gamma \left| \frac{x_{10}}{c} \right|^\delta + \mu \quad (\text{A.11})$$

correspond to periodic orbits of type 12. When $\delta < 1$ such fixed points exist only for $\mu > 0$. Note that this analysis predicts that periodic orbits of type 1 and type 12 will be present on opposite sides of the supergluing bifurcation at $\mu = 0$, in agreement with the numerical results in Fig. 4. The results for periodic orbits of type 1 and 12 provide a full description of the gluing bifurcation in two dimensions.

We next consider the map $P_1^{\text{glo}} \circ P_{31}^{\text{loc}} : S_3^{\text{in}} \rightarrow S_1^{\text{in}}$,

$$P_1^{\text{glo}} \circ P_{31}^{\text{loc}} : \begin{pmatrix} x_{10} \\ x_{20} \\ x_{30} \\ c \end{pmatrix} \rightarrow \begin{pmatrix} \gamma \left| \frac{x_{10}}{c} \right| x_{20} + \mu \\ c \\ \alpha_1 \left| \frac{c}{x_{10}} \right| x_{30} + \beta_1 c \left| \frac{x_{10}}{c} \right|^\delta \\ \alpha_2 \left| \frac{c}{x_{10}} \right| x_{30} + \beta_2 c \left| \frac{x_{10}}{c} \right|^\delta \end{pmatrix}. \tag{A.12}$$

We look for periodic orbits $(x_1^*(t), x_2^*(t), x_3^*(t), x_4^*(t))$ with period T and the symmetry property

$$(x_1^*(t + \frac{1}{2}T), x_2^*(t + \frac{1}{2}T), x_3^*(t + \frac{1}{2}T), x_4^*(t + \frac{1}{2}T)) = (x_3^*(t), x_4^*(t), x_1^*(t), x_2^*(t)).$$

A map (A.12) that maps $(x_{10}, x_{20}, x_{30}, x_{40}) \rightarrow (x_{30}, x_{40}, x_{10}, x_{20})$ corresponds to a time evolution through $\frac{1}{2}T$ (starting in S_3^{in} and ending in S_1^{in}) along a T -periodic orbit with this symmetry property. During this time the trajectory follows first the homoclinic orbit labeled 1 and then, over the next $\frac{1}{2}T$, the homoclinic orbit labeled 3. Thus, solutions to the equations

$$x_{30} = \gamma \left| \frac{x_{10}}{c} \right|^\delta x_{20} + \mu, \quad x_{10} = \alpha_1 \left| \frac{c}{x_{10}} \right| x_{30} + \beta_1 c \left| \frac{x_{10}}{c} \right|^\delta, \quad x_{20} = \alpha_2 \left| \frac{c}{x_{10}} \right| x_{30} + \beta_2 c \left| \frac{x_{10}}{c} \right|^\delta$$

correspond to periodic orbits of type 13. These equations may be reduced to the single equation

$$x_{10} = \alpha_1 \gamma \left| \frac{x_{10}}{c} \right|^{\delta-1} \left(\frac{\mu \alpha_2 |x_{10}/c|^{-1} + \beta_2 c |x_{10}/c|^\delta}{1 - \alpha_2 \gamma |x_{10}/c|^{\delta-1}} \right) + \mu \alpha_1 \left| \frac{x_{10}}{c} \right|^{-1} + \beta_1 c \left| \frac{x_{10}}{c} \right|^\delta \tag{A.13}$$

which may be simplified, using $x_{10} \ll c$ and the fact that $\delta < 1$, to give

$$\begin{aligned} x_{10} &= -\frac{\alpha_1}{\alpha_2} \left(\frac{\mu \alpha_2 |x_{10}/c|^{-1} + \beta_2 c |x_{10}/c|^\delta}{1 - (1/\alpha_2 \gamma) |x_{10}/c|^{1-\delta}} \right) + \mu \alpha_1 \left| \frac{x_{10}}{c} \right|^{-1} + \beta_1 c \left| \frac{x_{10}}{c} \right|^\delta \\ &\approx -\frac{\alpha_1}{\alpha_2} \left(\mu \alpha_2 \left| \frac{x_{10}}{c} \right|^{-1} + \beta_2 c \left| \frac{x_{10}}{c} \right|^\delta \right) \left(1 + \frac{1}{\alpha_2 \gamma} \left| \frac{x_{10}}{c} \right|^{1-\delta} \right) + \mu \alpha_1 \left| \frac{x_{10}}{c} \right|^{-1} + \beta_1 c \left| \frac{x_{10}}{c} \right|^\delta \\ &\approx -\frac{\alpha_1 \mu}{\alpha_2 \gamma} \left| \frac{x_{10}}{c} \right|^{-\delta}. \end{aligned} \tag{A.14}$$

We verify a posteriori that the approximation (A.14) has a solution $x_{10} \ll c$ provided μ is sufficiently small (see Fig. 18) and either $\mu > 0$ or $\mu < 0$, but not both.

Finally, we consider the map $P_1^{\text{glo}} \circ P_{41}^{\text{loc}} : S_4^{\text{in}} \rightarrow S_1^{\text{in}}$, given by

$$P_1^{\text{glo}} \circ P_{41}^{\text{loc}} : S_4^{\text{in}} \rightarrow S_1^{\text{in}} : \begin{pmatrix} x_{10} \\ x_{20} \\ x_{30} \\ -c \end{pmatrix} \rightarrow \begin{pmatrix} \gamma \left| \frac{x_{10}}{c} \right|^\delta x_{20} + \mu \\ c \\ \alpha_1 \left| \frac{c}{x_{10}} \right| x_{30} - \beta_1 c \left| \frac{x_{10}}{c} \right|^\delta \\ \alpha_2 \left| \frac{c}{x_{10}} \right| x_{30} - \beta_2 c \left| \frac{x_{10}}{c} \right|^\delta \end{pmatrix}. \tag{A.15}$$

We look for periodic orbits $(x_1^*(t), x_2^*(t), x_3^*(t), x_4^*(t))$ with period T and the symmetry property

$$(x_1^*(t + \frac{1}{4}T), x_2^*(t + \frac{1}{4}T), x_3^*(t + \frac{1}{4}T), x_4^*(t + \frac{1}{4}T)) = (-x_3^*(t), -x_4^*(t), x_1^*(t), x_2^*(t)).$$

A map (A.15) that maps $(x_{10}, x_{20}, x_{30}, x_{40}) \rightarrow (-x_{30}, -x_{40}, x_{10}, x_{20})$ corresponds to evolution through $\frac{1}{4}T$ (starting in S_4^{in} and ending on S_1^{in}) along a T -periodic orbit with this symmetry property. During this time the trajectory follows the homoclinic orbit labeled 1; over the next $\frac{1}{4}T$ it follows the homoclinic orbit 3, then 2 and then 4. Thus, solutions to the equations

$$-x_{30} = \gamma \left| \frac{x_{10}}{c} \right|^\delta x_{20} + \mu, \quad (\text{A.16})$$

$$x_{10} = \alpha_1 \left| \frac{c}{x_{10}} \right| x_{30} - \beta_1 c \left| \frac{x_{10}}{c} \right|^\delta, \quad (\text{A.17})$$

$$x_{20} = \alpha_2 \left| \frac{c}{x_{10}} \right| x_{30} - \beta_2 c \left| \frac{x_{10}}{c} \right|^\delta \quad (\text{A.18})$$

correspond to periodic orbits of type 1324. These equations may be reduced to a single equation for x_{10} given by (A.13) but with

$$(\alpha_1, \alpha_2, \beta_1, \beta_2) \rightarrow (-\alpha_1, -\alpha_2, -\beta_1, -\beta_2).$$

From Eq. (A.14), we now see that the equations for periodic orbits of types 13 and 1324 are identical. We expect, therefore, that periodic orbits of types 13 and 1324 coexist locally either for $\mu > 0$ or $\mu < 0$, but not for both (compare Fig. 18(a,b) with (c,d)). This is in agreement with the numerical results presented in Fig. 4.

In principle, one could also construct maps corresponding to other possible periodic orbits, such as periodic orbits of type 1323 or 123 which were shown numerically to be associated with the supergluing bifurcation. Unfortunately, this analysis requires the study of more complicated maps than those considered above: instead of a single map

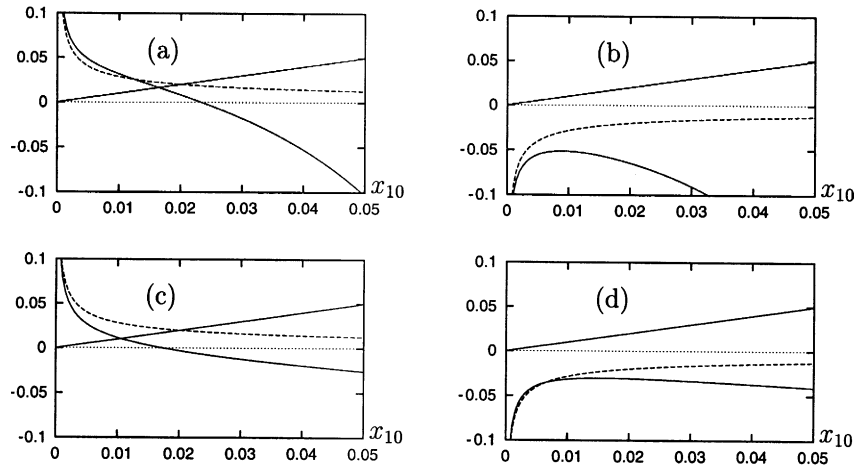


Fig. 18. Analysis of Eqs. (A.13) and (A.14). Here $c = 0.1$, $\delta = 0.5$, $\gamma = 1$, and (a) $\alpha_1 = 0.9, \alpha_2 = \beta_1 = \beta_2 = 1, \mu = -0.01$, (b) $\alpha_1 = 0.9, \alpha_2 = \beta_1 = \beta_2 = 1, \mu = 0.01$, (c) $\alpha_1 = -0.9, \alpha_2 = \beta_1 = \beta_2 = -1, \mu = -0.01$, (d) $\alpha_1 = -0.9, \alpha_2 = \beta_1 = \beta_2 = -1, \mu = 0.01$. The straight solid line is the lefthand side of (A.13), the other solid line is the right-hand side of (A.13), and the dashed line is the right-hand side of (A.14). Thus, solutions of Eq. (A.13) correspond to intersections of the solid lines, while solutions for the approximation correspond to intersections of the straight solid line with the dashed line.

from S_I^{in} to S_1^{in} , compositions of such maps would be required. An alternative approach is to consider the reduced map \tilde{P} for which we fix $x_2 = c$ in (A.7)

$$\tilde{P} : \begin{pmatrix} x_1 \\ x_3 \\ x_4 \end{pmatrix} \rightarrow \begin{pmatrix} \gamma \left| \frac{x_1}{c} \right|^\delta c + \mu \\ \alpha_1 \left| \frac{c}{x_1} \right| x_3 + \beta_1 \left| \frac{x_1}{c} \right|^\delta x_4 \\ \alpha_2 \left| \frac{c}{x_1} \right| x_3 + \beta_2 \left| \frac{x_1}{c} \right|^\delta x_4 \end{pmatrix}. \quad (\text{A.19})$$

This three-dimensional map is identical in form to Eq. (11) of Matthies [26], obtained for the Takens–Bogdanov bifurcation with D_3 symmetry. Matthies shows that a higher-dimensional generalization of a Smale horseshoe exists for this map, with the dynamics topologically conjugate to a shift on two symbols. By interpreting these results in the context of the Takens–Bogdanov bifurcation with D_3 , he is able to show that the result corresponds to a subshift of finite type (as defined in [50]) encoding the itinerary along the symmetry-related homoclinic orbits. The numerical results presented in the text show that the supergluing bifurcation gives birth to unstable periodic orbits of many different types, and these are perhaps related to a subshift similar to that found by Matthies. A more detailed analysis of the map \tilde{P} for the supergluing bifurcation would be of great interest not only to the consideration of the resonantly forced Hopf bifurcation with D_4 symmetry, but also the general problem of the Takens–Bogdanov bifurcation with D_4 symmetry (e.g., [25,51–53]).

References

- [1] G. Dangelmayr, E. Knobloch, On the Hopf bifurcation with broken $O(2)$ symmetry, in: W. Güttinger, G. Dangelmayr (Eds.), *The Physics of Structure Formation*, Springer, Berlin, 1987, pp. 387–393.
- [2] G. Dangelmayr, E. Knobloch, Hopf bifurcation with broken circular symmetry, *Nonlinearity* 4 (1991) 399–427.
- [3] R. Lauterbach, M. Roberts, Heteroclinic cycles in dynamical systems with broken spherical symmetry, *J. Diff. Eq.* 100 (1992) 22–48.
- [4] E. Knobloch, System symmetry breaking and Shil’nikov dynamics, in: J. Chadam, M. Golubitsky, W. Langford, B. Wetton (Eds.), *Pattern Formation: Symmetry Methods and Applications*. American Mathematical Society, Providence, 1996, pp. 271–279.
- [5] P. Hirschberg, E. Knobloch, Complex dynamics in the Hopf bifurcation with broken translation symmetry, *Physica D* 92 (1996) 56–78.
- [6] A.S. Landsberg, E. Knobloch, Oscillatory bifurcation with broken translation symmetry, *Phys. Rev. E* 53 (1996) 3579–3600.
- [7] J. Moehlis, E. Knobloch, Forced symmetry breaking as a mechanism for bursting, *Phys. Rev. Lett.* 80 (1998) 5329–5332.
- [8] J. Moehlis, E. Knobloch, Bursts in oscillatory systems with broken D_4 symmetry, *Physica D* 135 (2000) 263–304.
- [9] J.M. Gambaudo, Perturbation of a Hopf bifurcation by an external time-periodic forcing, *J. Diff. Eq.* 57 (1985) 172–199.
- [10] A. Chiffaudel, S. Fauve, Strong resonance in forced oscillatory convection, *Phys. Rev. A* 35 (1987) 4004–4007.
- [11] H. Riecke, J.D. Crawford, E. Knobloch, Time-modulated oscillatory convection, *Phys. Rev. Lett.* 61 (1988) 1942–1945.
- [12] D. Walgraef, External forcing of spatio-temporal patterns, *Europhys. Lett.* 7 (1988) 485–491.
- [13] W. Vance, J. Ross, A detailed study of a forced chemical oscillator: Arnold’s tongues and bifurcation sets, *J. Chem. Phys.* 91 (1989) 7654–7670.
- [14] H. Riecke, M. Silber, L. Kramer, Temporal forcing of small-amplitude waves in anisotropic systems, *Phys. Rev. E* 49 (1994) 4100–4113.
- [15] I. Rehberg, S. Rasenat, J. Fineberg, M. de la Torre Juárez, V. Steinberg, Temporal modulation of traveling waves, *Phys. Rev. Lett.* 61 (1988) 2449–2452.
- [16] S.G.K. Tennakoon, C.D. Andereck, J.J. Hegseth, H. Riecke, Temporal modulation of traveling waves in the flow between rotating cylinders with broken azimuthal symmetry, *Phys. Rev. E* 54 (1996) 5053–5065.
- [17] M. de la Torre Juárez, I. Rehberg, Four-wave resonance in electrohydrodynamic convection, *Phys. Rev. A* 42 (1990) 2096–2100.
- [18] C. Elphick, G. Iooss, E. Tirapegui, Normal form reduction for time-periodically driven differential equations, *Phys. Lett. A* 120 (1987) 459–463.
- [19] C. Elphick, E. Tirapegui, M.E. Brachet, P. Coulet, G. Iooss, A simple global characterization for normal forms of singular vector fields, *Physica D* 29 (1987) 95–127 (Addendum, *Physica D* 32 (1988) 488).
- [20] J.W. Swift, Hopf bifurcation with the symmetry of the square, *Nonlinearity* 1 (1988) 333–377.

- [21] E. Doedel, A. Champneys, T. Fairgrieve, Y. Kuznetsov, B. Sandstede, X. Wang, AUTO 97: continuation and bifurcation software for ordinary differential equations; available via FTP from directory pub/doedel/auto at ftp.cs.concordia.ca, 1997.
- [22] J. Moehlis, Forced Symmetry-Breaking as a Mechanism for Bursting, Ph.D. Thesis, University of California, Berkeley, CA, 2000.
- [23] J. Guckenheimer, P. Holmes, Nonlinear Oscillations, Dynamical Systems, and Bifurcations of Vector Fields, Springer, Berlin, 1983.
- [24] A.M. Rucklidge, Chaos in a low-order model of magnetoconvection, *Physica D* 62 (1993) 323–337.
- [25] A.M. Rucklidge, Global bifurcations in the Takens–Bogdanov normal form with D_4 symmetry near the $O(2)$ limit, Preprint, 2000.
- [26] K. Matthies, A subshift of finite type in the Bogdanov–Takens bifurcation with D_3 symmetry, *Doc. Math. J. DMV* 4 (1999) 463–485.
- [27] M. Golubitsky, I. Stewart, D.G. Schaeffer, Singularities and Groups in Bifurcation Theory, Vol. II, Springer, Berlin, 1988.
- [28] J.P. Gollub, S.V. Benson, Many routes to turbulent convection, *J. Fluid Mech.* 100 (1980) 449–470.
- [29] P. Bergé, Y. Pomeau, C. Vidal, Order Within Chaos: Towards a Deterministic Approach to Turbulence, Wiley, New York, 1984.
- [30] R.E. Ecke, I.G. Kevrekidis, Interactions of resonances and global bifurcations in Rayleigh–Bénard convection, *Phys. Lett. A* 131 (1988) 344–352.
- [31] I.G. Kevrekidis, R. Rico-Martinez, R.E. Ecke, R.M. Farber, A.S. Lapedes, Global bifurcations in Rayleigh–Bénard convection. Experiments, empirical maps and numerical bifurcation analysis, *Physica D* 71 (1994) 342–362.
- [32] I. Schreiber, M. Marek, Transition to chaos via two-torus in coupled reaction–diffusion cells, *Phys. Lett. A* 91 (1982) 263–266.
- [33] V. Franceschini, C. Tebaldi, Breaking and disappearance of tori, *Commun. Math. Phys.* 94 (1984) 317–329.
- [34] J. Curry, J. Yorke, A transition from Hopf bifurcation to chaos: computer experiments on maps in \mathbb{R}^2 , The structure of attractors in dynamical systems, *Lecture Notes in Mathematics*, Vol. 668, Springer, Berlin, 1978, pp. 48–68.
- [35] D.G. Aronson, M.A. Chory, G.R. Hall, R.P. McGehee, Bifurcations from an invariant circle for two-parameter families of maps of the plane: a computer-assisted study, *Commun. Math. Phys.* 83 (1982) 303–354.
- [36] D.G. Aronson, M.A. Chory, G.R. Hall, R.P. McGehee, A discrete dynamical system with subtly wild behavior, in: P.J. Holmes (Ed.), *New Approaches to Nonlinear Problems in Dynamics*, Society for Industrial and Applied Mathematics, Philadelphia, 1980, pp. 339–359.
- [37] A. Ben-Mizrachi, I. Procaccia, Wrinkling of mode-locked tori in the transition to chaos, *Phys. Rev. A* 31 (1985) 3990–3992.
- [38] C. Grebogi, E. Ott, J.A. Yorke, Chaotic attractors in crisis, *Phys. Rev. Lett.* 48 (1982) 1507–1510.
- [39] C. Grebogi, E. Ott, J.A. Yorke, Crises, sudden changes in chaotic attractors, and transient chaos, *Physica D* 7 (1983) 181–200.
- [40] E. Knobloch, J. Moehlis, Bursting mechanisms for hydrodynamical systems, in: M. Golubitsky, D. Luss, S.H. Strogatz (Eds.), *Pattern Formation in Continuous and Coupled Systems: A Survey Volume*, Series: IMA Volumes in Mathematics and its Applications, Vol. 115, Springer, Berlin, 1999, pp. 157–174.
- [41] E. Knobloch, J. Moehlis, Burst mechanisms in hydrodynamics, in: L. Debnath, D. Riahi (Eds.), *Nonlinear Instability, Chaos, and Turbulence*, Vol. II, Computational Mechanics Publications, Southampton, 2000, pp. 237–287.
- [42] Y. Pomeau, P. Manneville, Intermittent transition to turbulence in dissipative dynamical systems, *Commun. Math. Phys.* 74 (1980) 189–197.
- [43] A. Steindl, H. Troger, One and two-parameter bifurcations to divergence and flutter in the three-dimensional motions of a fluid conveying viscoelastic tube with D_4 symmetry, *Nonlinear Dynam.* 8 (1995) 161–178.
- [44] A.K. Bajaj, C.N. Folley, Three-dimensional dynamics of a continuous cantilever tube conveying a pulsatile flow, *Z. Angew. Math. Mech.* 76 (no. 2 Suppl.) (1996) 547–550.
- [45] Z.C. Feng, P.R. Sethna, Symmetry-breaking bifurcations in resonant surface waves, *J. Fluid Mech.* 199 (1989) 495–518.
- [46] F. Simonelli, J.P. Gollub, Surface wave mode interactions: effects of symmetry and degeneracy, *J. Fluid Mech.* 199 (1989) 471–494.
- [47] M. Silber, E. Knobloch, Parametrically excited surface waves in square geometry, *Phys. Lett. A* 137 (1989) 349–354.
- [48] M. Nagata, Nonlinear Faraday resonance in a box with a square base, *J. Fluid Mech.* 209 (1989) 265–284.
- [49] M. Nagata, Chaotic behaviour of parametrically excited surface waves in square geometry, *Eur. J. Mech. B* 10 (no. 2 Suppl.) (1991) 61–66.
- [50] M.J. Field, Isotopy and stability of equivariant diffeomorphisms, *Proc. London Math. Soc.* 46 (1983) 487–516.
- [51] D. Armbruster, J. Guckenheimer, S. Kim, Chaotic dynamics in systems with square symmetry, *Phys. Lett. A* 140 (1989) 416–420.
- [52] D. Armbruster, Codimension 2 bifurcation in binary convection with square symmetry, in: F.H. Busse, L. Kramer (Eds.), *Nonlinear Evolution of Spatio-temporal Structures in Dissipative Continuous Systems*, Plenum Press, New York, 1990, pp. 385–398.
- [53] D. Armbruster, Square and almost square symmetry in binary convection, *Eur. J. Mech. B* 10 (no. 2 Suppl.) (1991) 7–12.